ELECTRONIC SUPPLEMENTARY INFORMATION

Photo-controllable Binding and Release of $HP_2O_7^{3-}$ Using an Azobenzene based Smart Macrocycle

Shenglun Xiong, Yi Zhang, Yunqi Jiang, Fei Wang, Wei Zhou, Aimin Li, Qinpeng Zhang, Qiuan Wang, and Qing He*

State Key Laboratory of Chemo/Biosensing and Chemometrics, College of Chemistry and Chemical Engineering, Hunan University, Changsha 410082, P. R. China.

* Correspondence: Qing He (heqing85@hnu.edu.cn)

Contents

1. General experimental

All solvents and chemicals used were purchased from Sigma–Aldrich, TCI, Energy–Chemical, or Acros and used without further purification. TLC analyses were carried out using Sorbent Technologies silica gel (200-300 mesh) sheets. ^{1}H and ^{13}C NMR spectra were recorded on Bruker AVANCE 400 spectrometers and the spectroscopic solvents were purchased from Cambridge Isotope Laboratories or Sigma–Aldrich. Either residual solvent peak or tetramethylsilane (TMS) was used as an internal reference. The chemical shifts are expressed in δ (ppm). High–resolution mass spectra (HRMS) were recorded on a Bruker Apex–Q IV FTMS mass spectrometer using ESI (electrospray ionization). X–ray crystallographic analyses were carried out on a Brucker D8 Venture diffractometer using a *μ*–focused Cu Kα radiation source (λ = 1.54184 Å). Theoretical calculations for evaluating the stability of structures were carried out with the Gaussian 09 suite[1] of programs using the X3LYP density functional.[2] Structural optimization was performed using a 6–31G* basis set while single–point energy was calculated with a 6–31++g** basis set. Complexation energies were corrected for basis set superposition error (BSSE) using the counterpoise correction method.[3, 4] As for UV-vis spectrum calculations, the DFT calculations were performed under Gaussian 09 suite[1] of programs using the PBE1PBE density functional.[2] Structural optimization was performed using a 6–31G* basis set while UV-vis spectrum was calculated with a 6–311g* basis set.

2. Synthesis

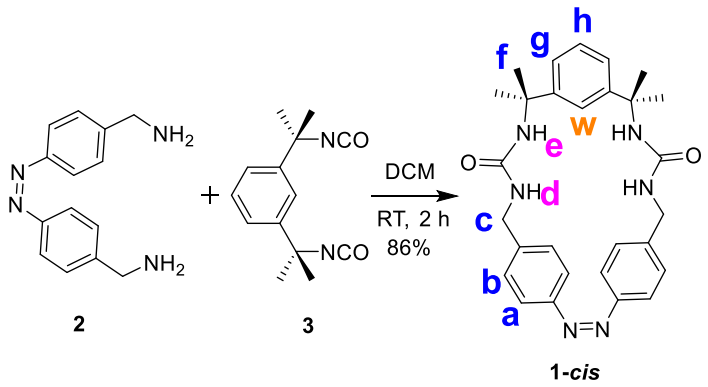

Scheme S1. Synthesis of **1-*cis*.**

Compound **2** (**2-trans**) was readily prepared according to the reported method.[5]

Synthesis of 1-*cis*

A solution of **2-*trans*** (349 mg, 1.45 mmol) in DCM (500 mL) was subjected to irradiation with 365-370 nm light until the photostationary state (PSS) was achieved. Then the resulting **2-*cis*** solution and the other solution of **3** (355 mg, 1.45 mmol) in DCM (500 mL) were added dropwise in parallel into a three-necked flask (2 L) for 2 h under N_2 atmosphere at room temperature. After completion of the addition, the mixture was stirred for one more hour. Subsequently, the reaction solution was concentrated and the resulting residue was subjected to chromatography (SiO_2: 200-300 mesh) using DCM/MeOH (20/1, V/V) as the eluent. Pure product **1-*cis*** (604 mg, 1.35 mmol) was obtained

as orange solid in 86% yield. ^{1}H NMR (400 MHz, DMSO-d_6) δ (ppm) 7.34 (s, 1H, ArH), 7.19 - 7.15 (m, 3H, ArH), 7.13 (d, *J* = 8.4 Hz, 4H, ArH), 6.76 (d, *J* = 8.4 Hz, 4H, ArH), 6.26 (t, *J* = 6.4 Hz, 2H, NH), 6.23 (s, 2H, NH), 4.07 (d, *J* = 6.4 Hz, 4H, CH_2), 1.50 (s, 12H, CH_3). ^{13}C NMR (100 MHz, DMSO-d_6) δ (ppm) 157.3, 151.7, 148.6, 140.6, 127.4, 122.7, 120.6, 119.7, 54.5, 42.2, 29.6. HRMS (ESI) m/z 485.2660 $[M + H^+]^+$ calcd for $C_{28}H_{33}N_6O_2^+$, found 485.2644; 502.2925 $[M + NH_4^+]^+$ calcd for $C_{28}H_{36}N_7O_2^+$, found 502.2909; 507.2479 $[M + Na^+]^+$ calcd for $C_{28}H_{32}N_6O_2Na^+$, found 507.2461; 991.5066 $[2M + Na^+]^+$ calcd for $C_{56}H_{64}N_{12}O_4Na^+$, found 991.5029; 483.2514 $[M - H^+]^-$ calcd for $C_{28}H_{31}N_6O_2^-$, found 483.2509; 519.2281 $[M + Cl^-]^-$ calcd for $C_{28}H_{32}ClN_6O_2^-$, found 519.2275; 967.5101 $[2M - H^+]^-$ calcd for $C_{56}H_{63}N_{12}O_4^-$, found 967.5096; 1143.7485 $[M + 2TBA^+ + HP_2O_7^{3-}]^-$ calcd for $C_{56}H_{63}N_{12}O_4^-$, found 1143.7489; 902.4716 $[M + H^+ + TBA^+ + HP_2O_7^{3-}]^-$ calcd for $C_{56}H_{63}N_{12}O_4^-$, found 902.4724.

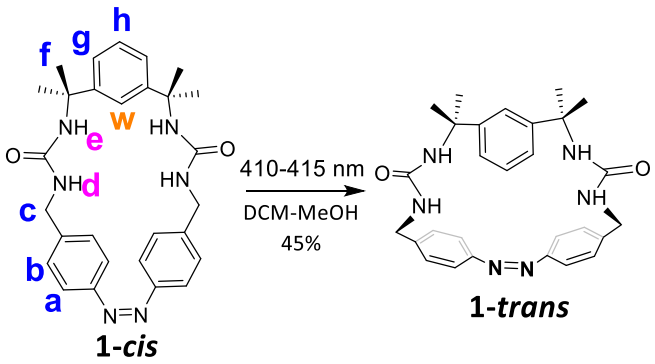

Scheme S2. Synthesis of **1-*trans*.**

Synthesis of 1-*trans*

1-*cis* (200 mg) was suspended in DCM (450 mL) and was added methanol (3 mL) dropwise until all the solid was dissolved. Then the solution was irradiated with 410-415 nm light to the photostationary state (PSS), a lot of orange-red solid was precipitated. After the precipitates were filtered and washed with a small amount of CH_2Cl_2, pure **1-*trans*** (89 mg) was obtained in 45% yield. ^{1}H NMR (400 MHz, DMSO-d_6) δ (ppm) 7.83 (brs, 4H, Azo-H), 7.47 (d, *J* = 8.0 Hz, 4H, Azo-H), 6.77 (s, 1H, ArH), 6.27 (t, *J* = 6.3 Hz, 2H, NH), 5.91 (s, 2H, NH), 5.86 - 5.76 (m, 1H, ArH), 5.50 (d, *J* = 7.7 Hz, 2H, ArH), 4.04 (d, *J* = 6.9 Hz, 4H, CH_2), 1.31 (brs, 12H, CH_3). ^{13}C NMR (100 MHz, DMSO-d_6) δ (ppm) 157.8, 152.0, 147.1, 144.1, 130.1, 126.4, 122.7, 121.5, 121.1, 56.0, 44.5.

Note: As we known, it is usually difficult to separate one isomer from the other one of the azobenzene derivative. To achieve this goal, the solvent utilized for this reaction was carefully optimized. Since in our current case, the *cis* isomer was not able to completely (or 100%) transform into its **trans** isomer. A mixture of isomers was always obtained. After careful optimization of the solvent, we found that **1-cis** was soluble in a mixture of DCM and MeOH (150:1, v/v) but **1-trans**

was almost insoluble in the same solvent system. As a result, upon irradiation of a solution of **1-cis** in a mixture of DCM and MeOH (150:1, v/v), abundant precipitates occurred within 5 min, which were evidenced to be pure **1-trans**. Meanwhile, different wavelength irradiation sources were used for photoisomerization (Fig. S1). Thus, 410-415 nm light proves the best *cis-trans* irradiation source.

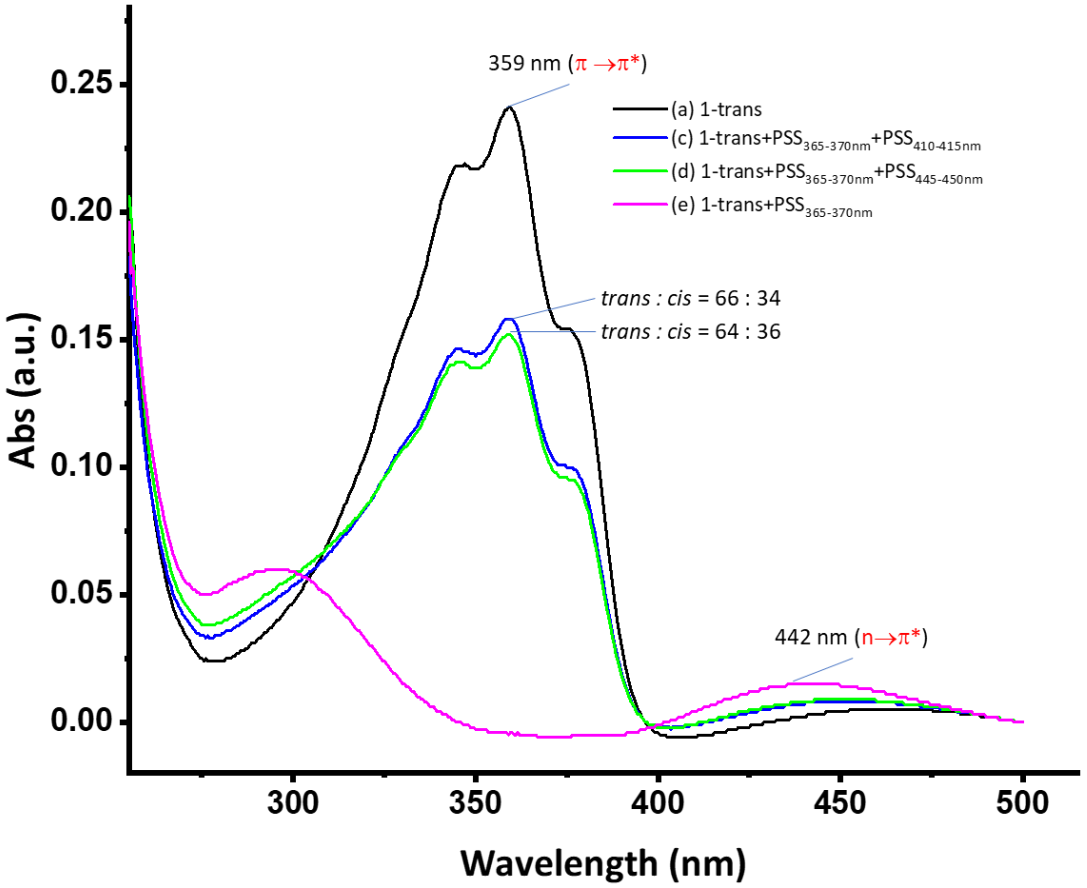

Fig. S1. Optimization of the irradiation source for the ***1-cis*⟶*1-trans*** photoisomerization.

3. HRMS Spectra and NMR Spectra

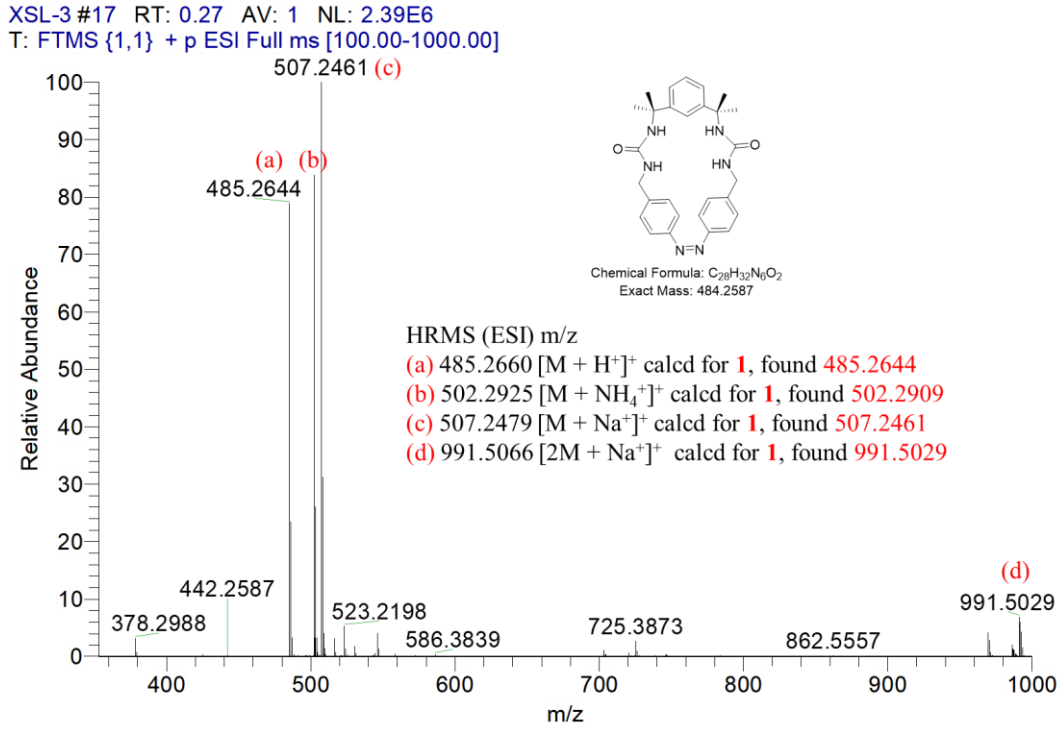

Fig. S2. HRMS (ESI, positive mode) of compound **1**.

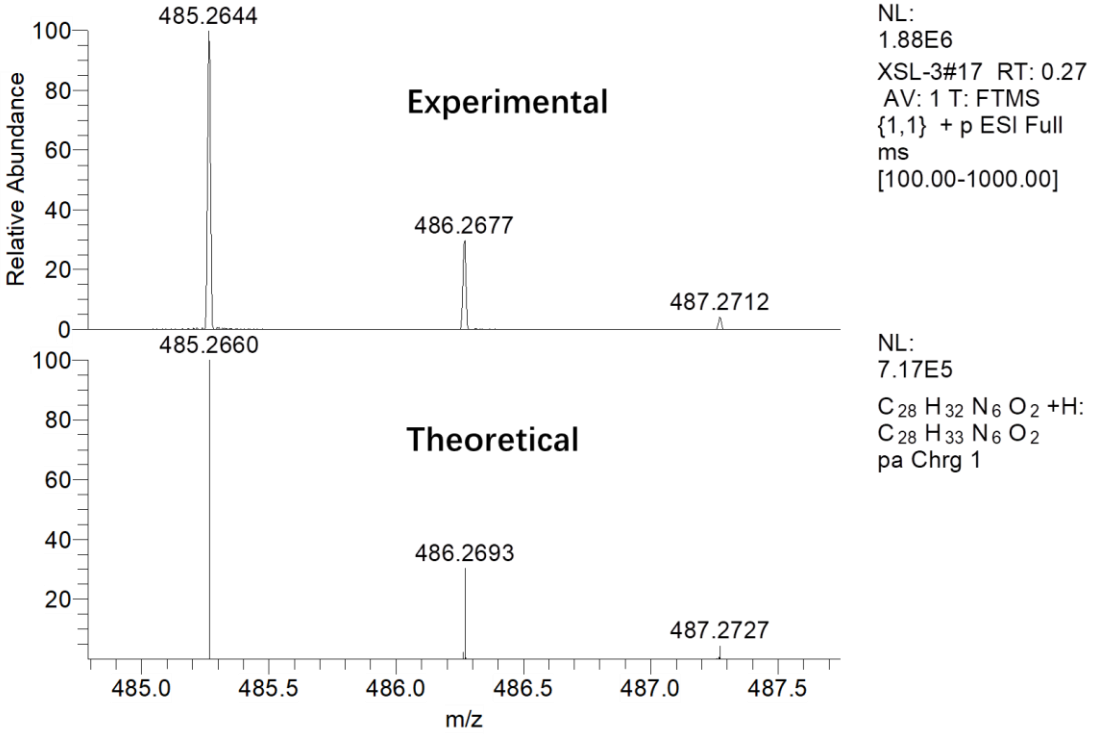

Fig. S3. Expanded ESI mass spectrum of compound **1**, displaying the peak of $[\mathbf{1} + H^+]^+$.

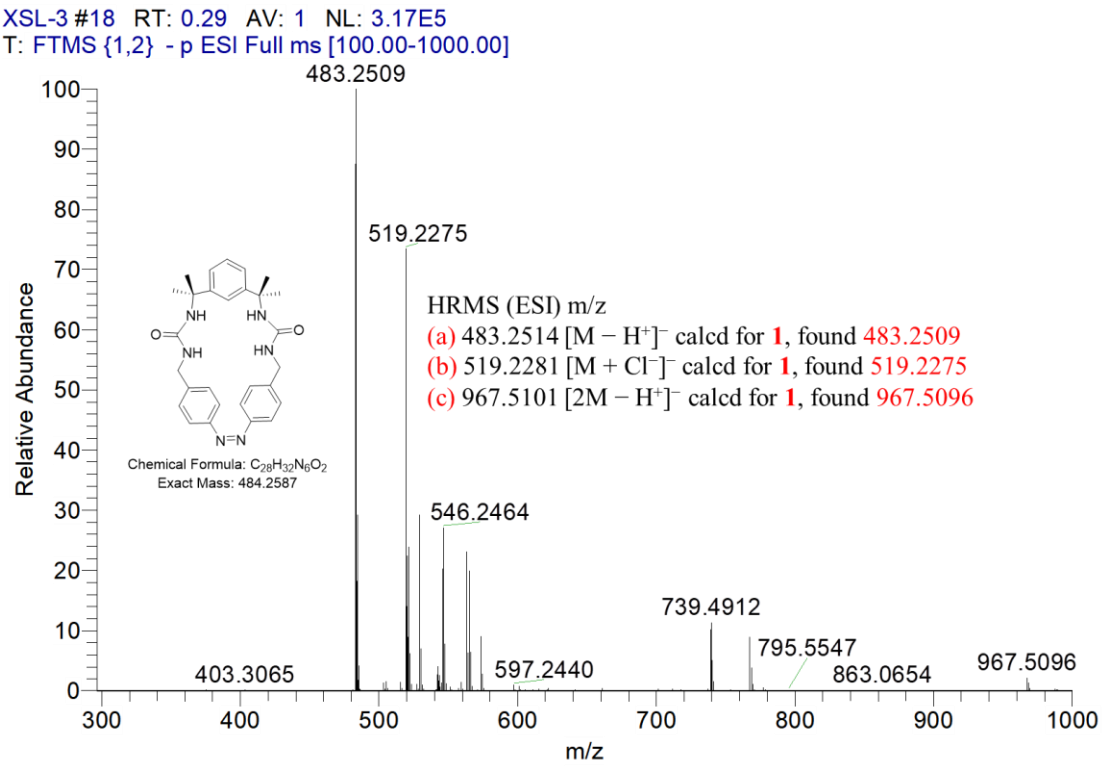

Fig. S4. HRMS (ESI, negative mode) of compound **1**.

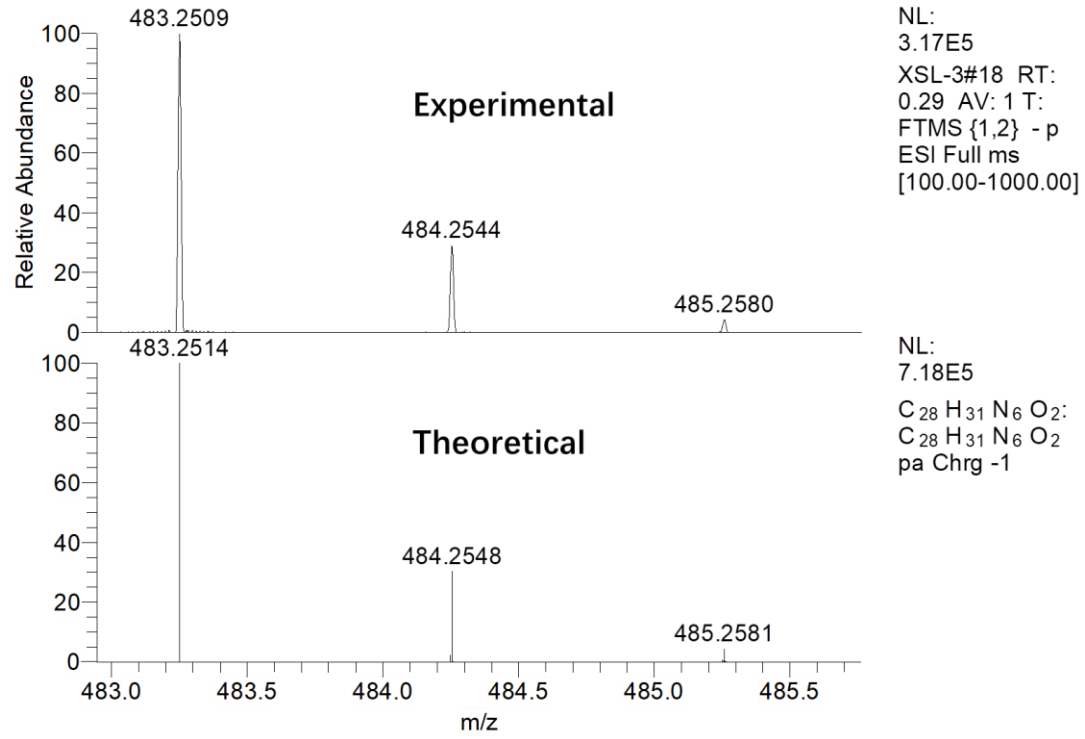

Fig. S5. Expanded ESI mass spectrum of compound **1**, displaying the peak of [**1** – H^+]$^-$.

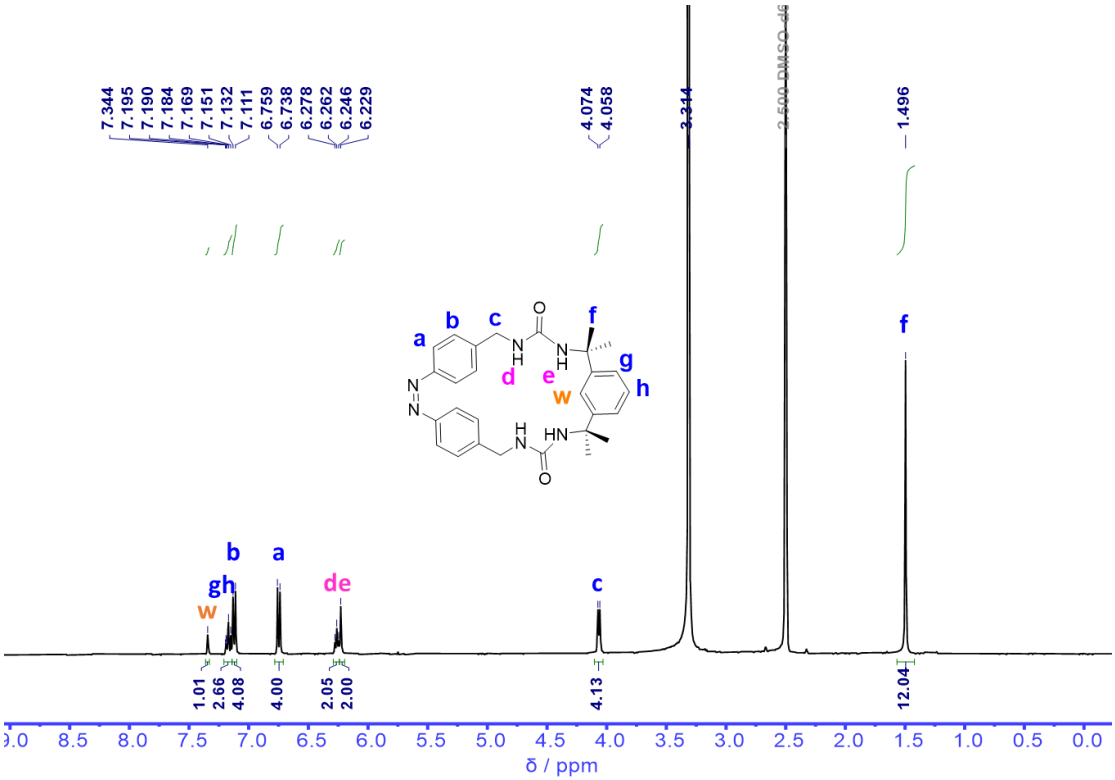

Fig. S6. ^{1}H NMR spectrum of **1-*cis*** recorded in DMSO-d_6 at 298 K.

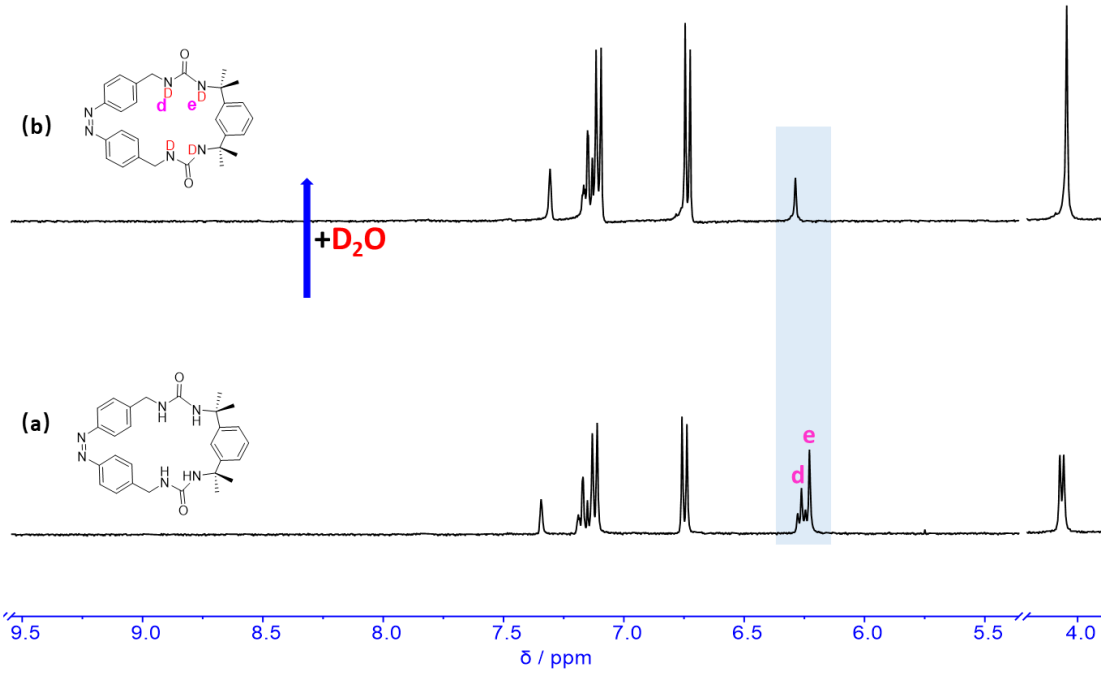

Fig. S7. Partial ^{1}H NMR spectra of **1-*cis*** (a) before and (b) after addition of D_2O recorded in DMSO-d_6 at 298 K.

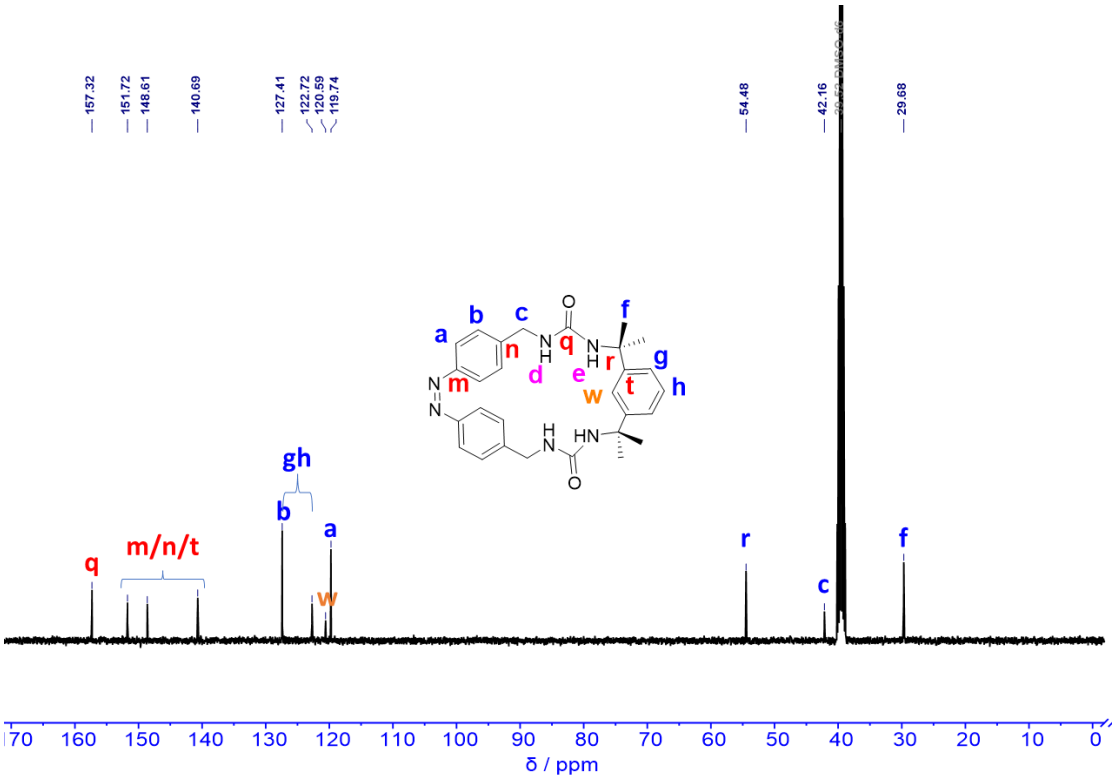

Fig. S8. ^{13}C NMR spectrum of **1-*cis*** recorded in DMSO-d_6 at 298 K.

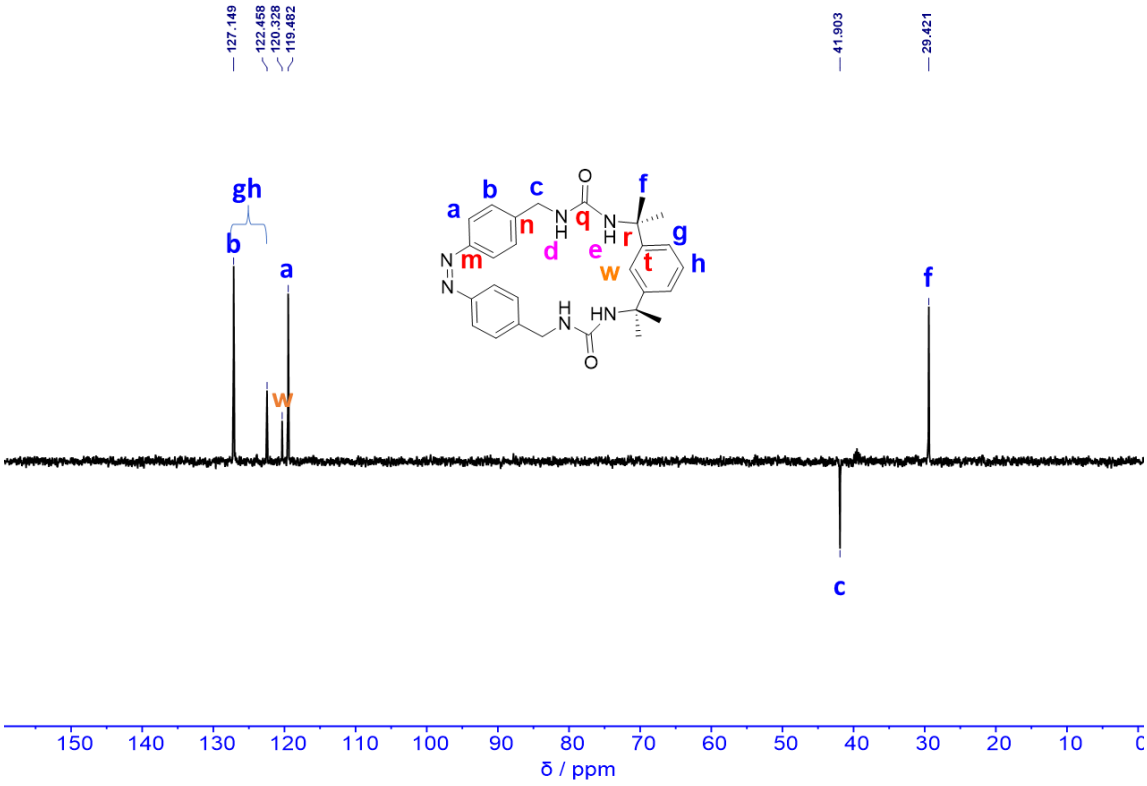

Fig. 9. DEPT135 spectrum of **1-*cis*** recorded in DMSO-d_6 at 298 K.

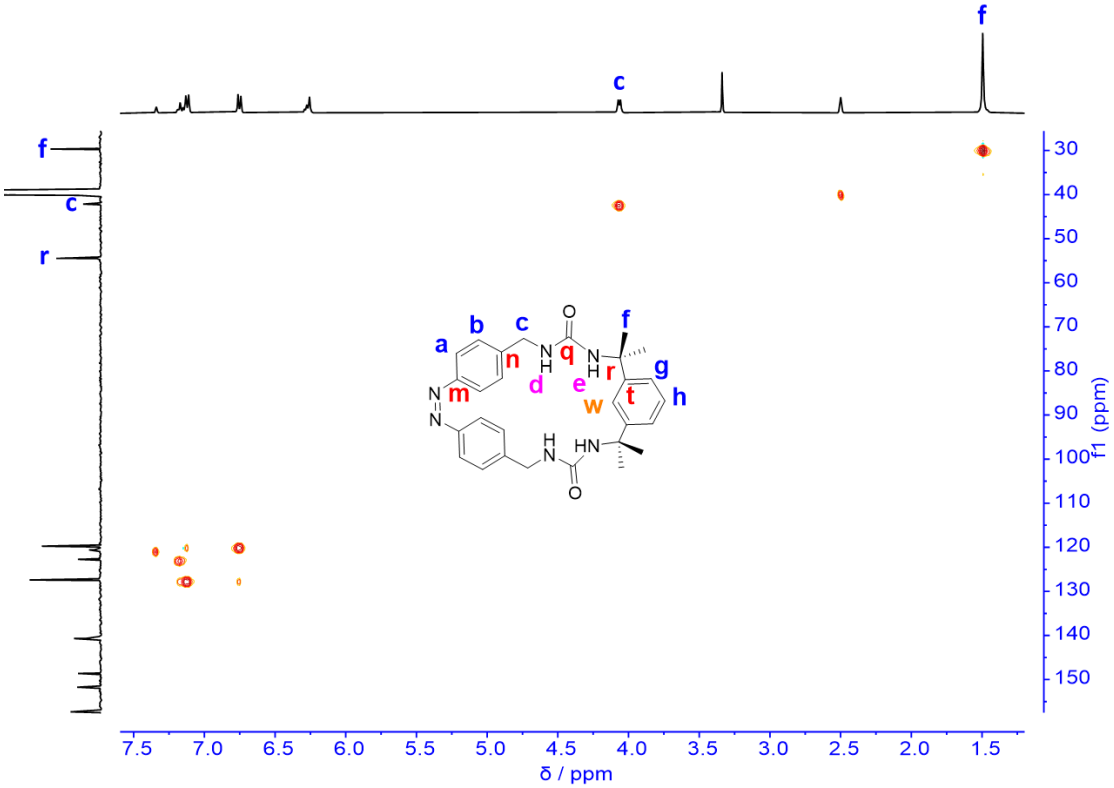

Fig. S10. HSQC (^{1}H-^{13}C) spectrum of **1-*cis*** recorded in DMSO-d_6 at 298 K.

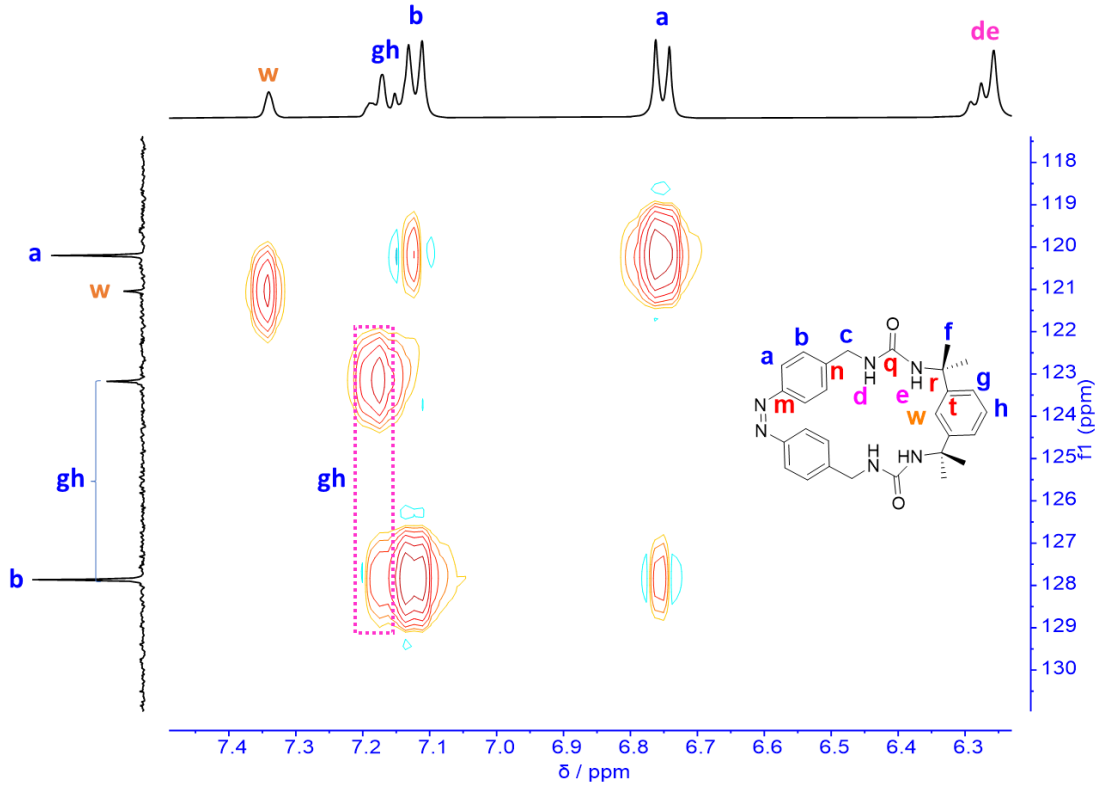

Fig. S11. Expanded HSQC (^{1}H-^{13}C) spectrum of **1-*cis*** recorded in DMSO-d_6 at 298 K.

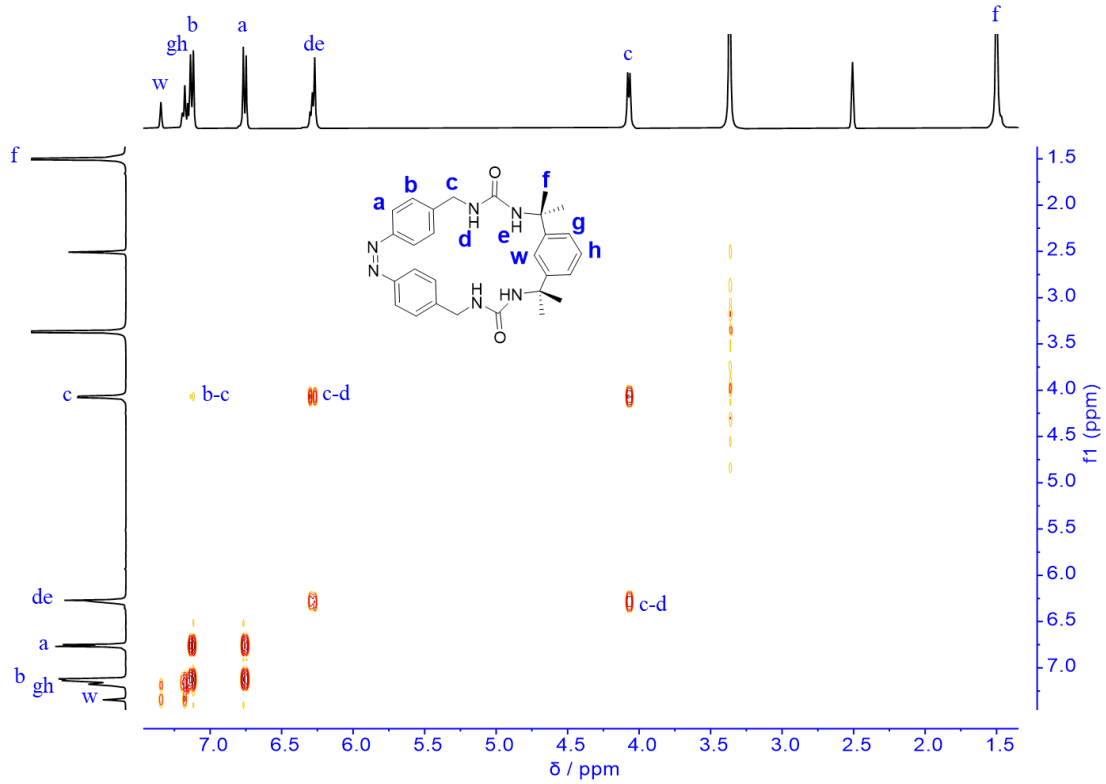

Fig. S12. ^{1}H-^{1}H COSY spectrum of **1-*cis*** recorded in DMSO-d_6 at 298 K.

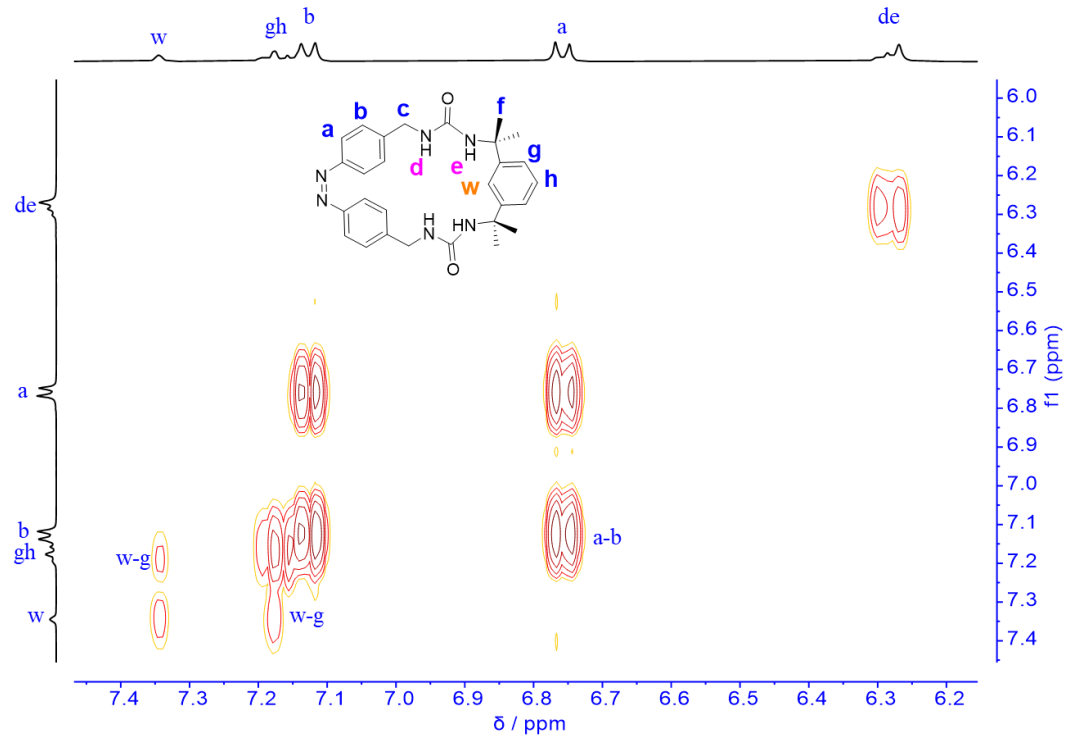

Fig. S13. Expanded ^{1}H-^{1}H COSY spectrum of **1-*cis*** recorded in DMSO-d_6 at 298 K.

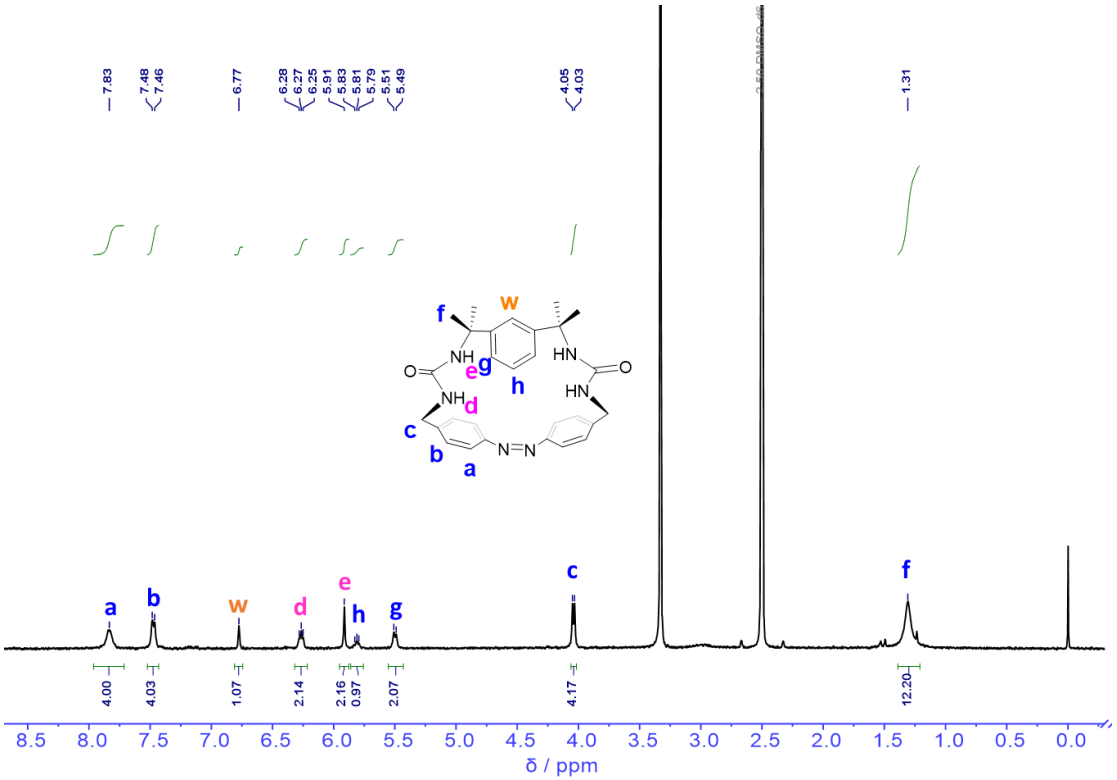

Fig. S14. ^{1}H NMR spectrum of **1-*trans*** recorded in DMSO-d_6 at 298 K.

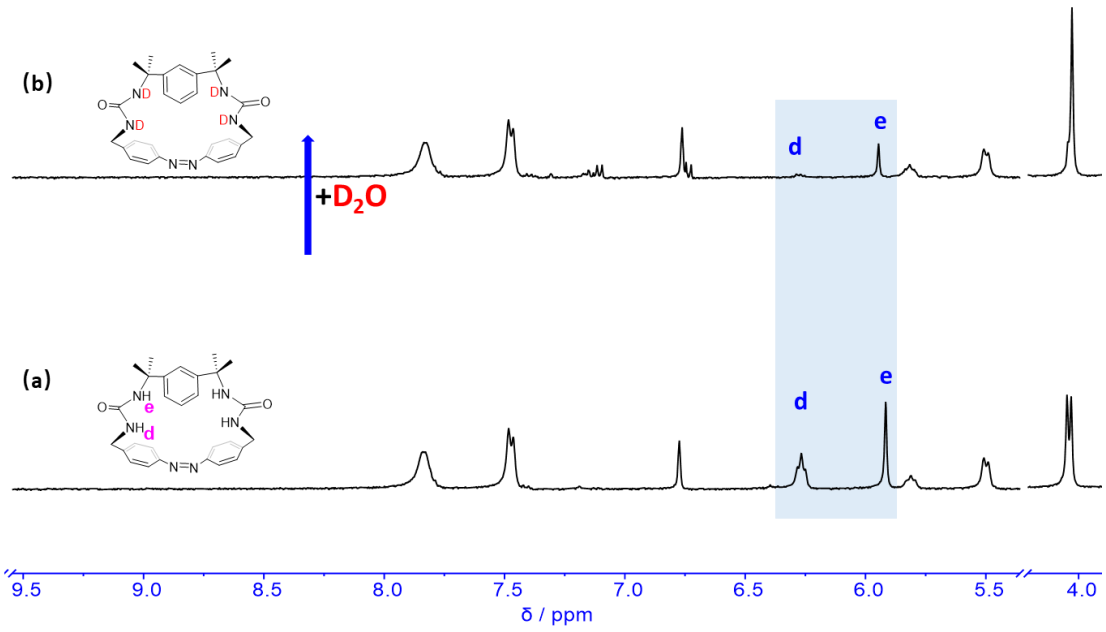

Fig. S15. Partial ^{1}H NMR spectra of **1-*trans*** (a) before and (b) after addition of D_2O recorded in DMSO-d_6 at 298 K.

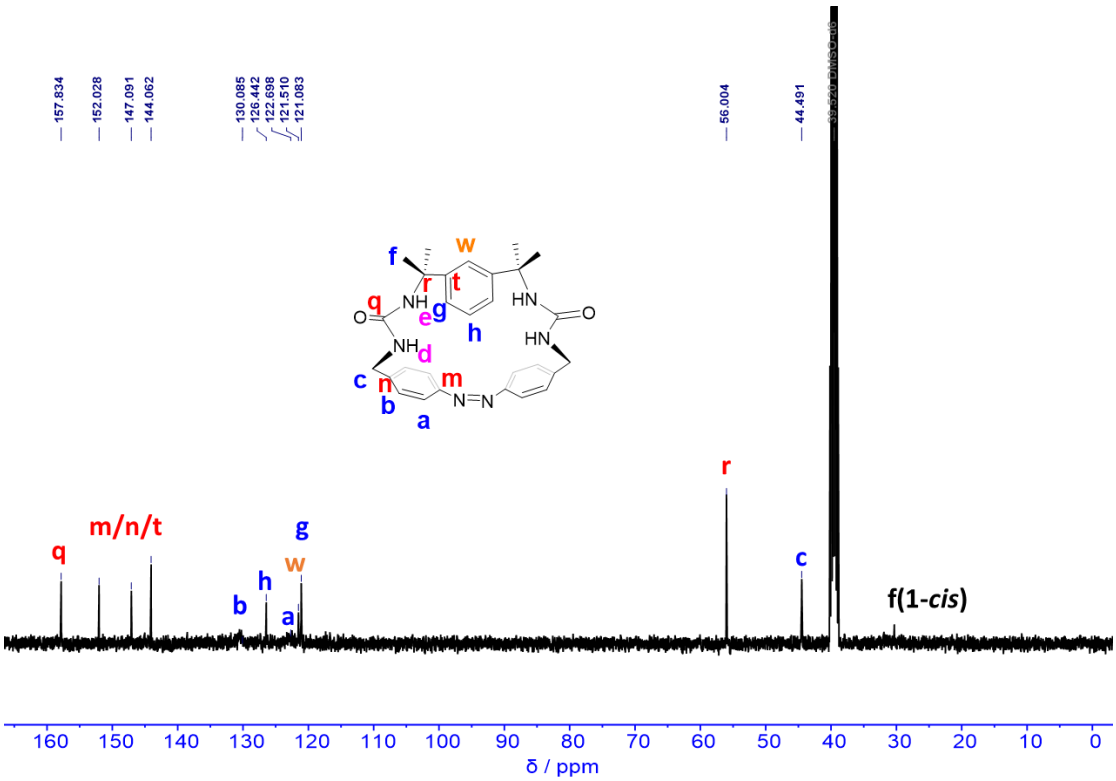

Fig. S16. ^{13}C NMR spectrum of **1-*trans*** recorded in DMSO-d_6 at 298 K.

`

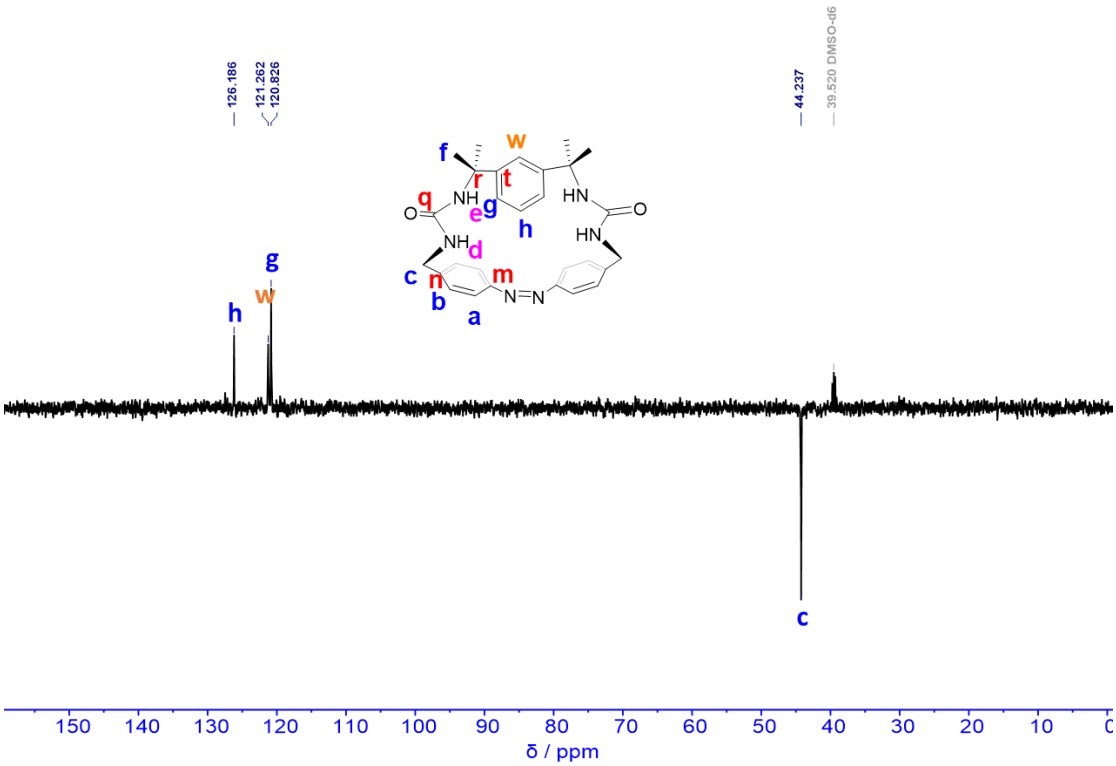

Fig. S17. DEPT135 spectrum of **1-*trans*** recorded in DMSO-d_6 at 298 K.

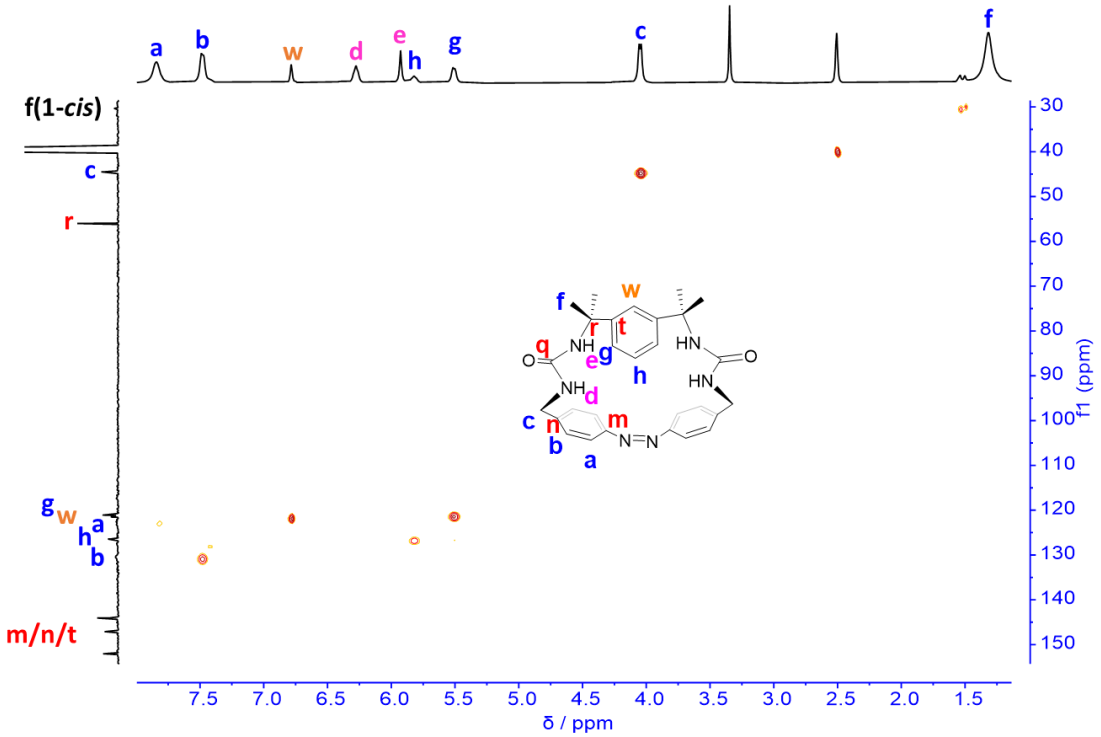

Fig. S18. HSQC (^{1}H-^{13}C) spectrum of **1-*trans*** recorded in DMSO-d_6 at 298 K.

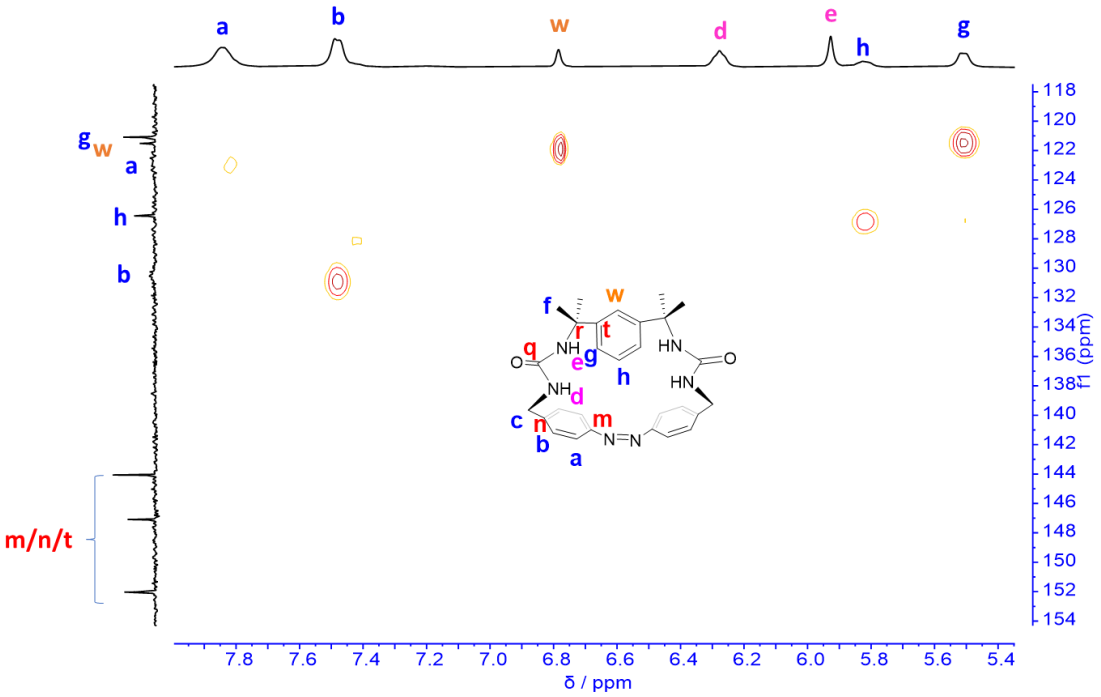

Fig. S19. Expanded HSQC (^{1}H-^{13}C) spectrum of **1-*trans*** recorded in DMSO-d_6 at 298 K.

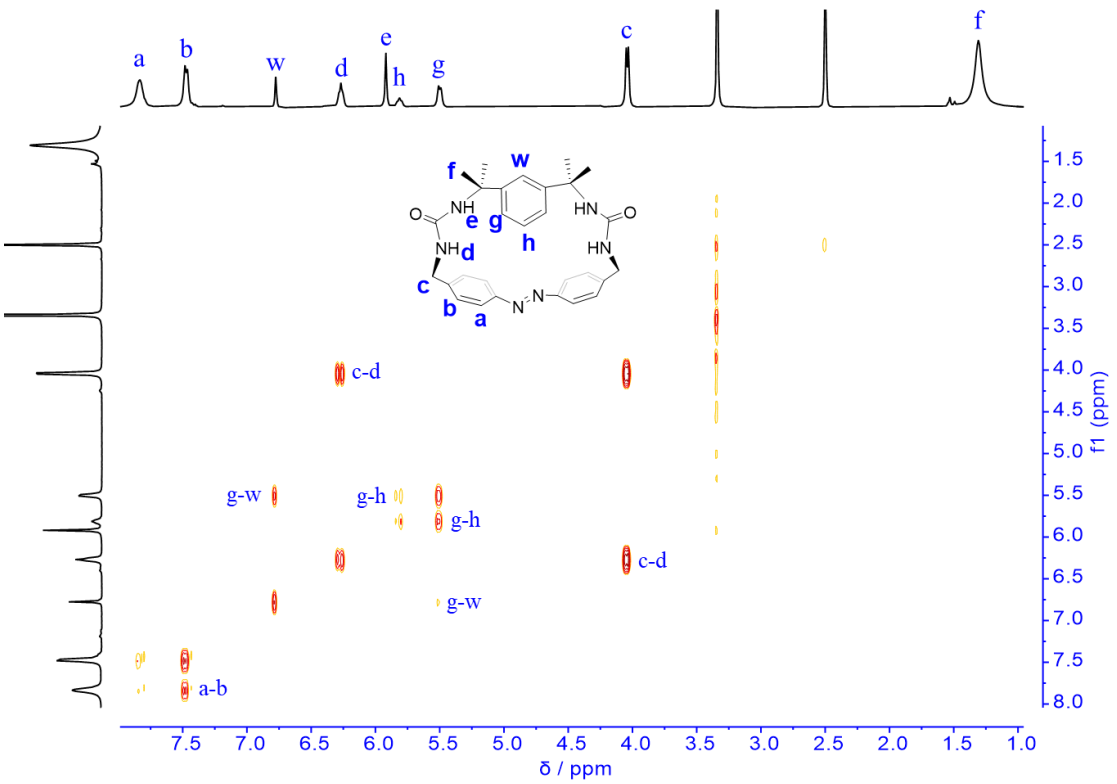

Fig. S20. ^{1}H-^{1}H COSY spectrum of **1-*trans*** recorded in DMSO-d_6 at 298 K.

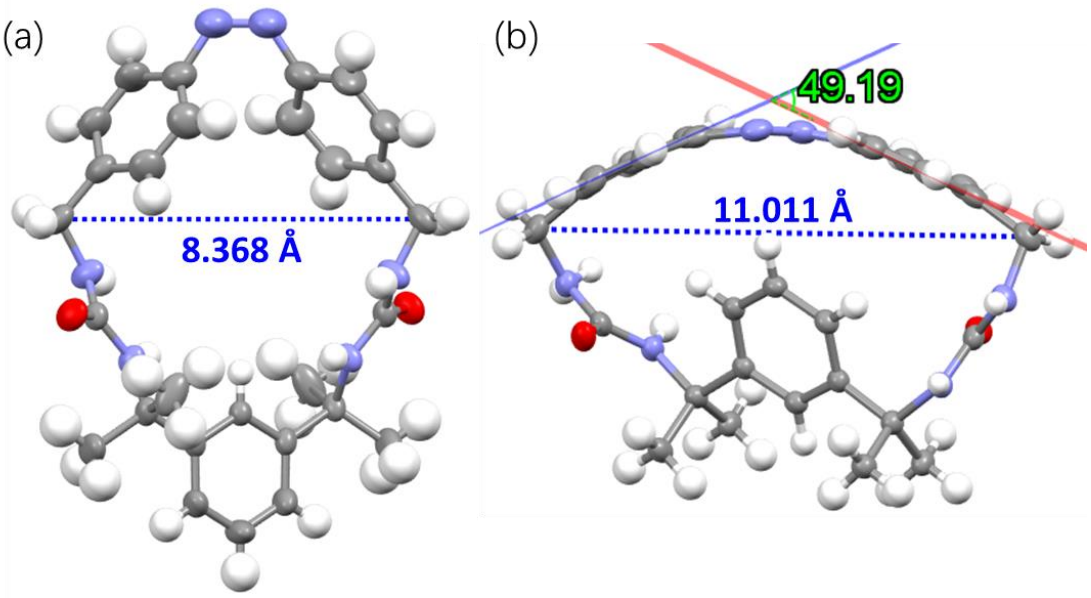

Fig. S21. X–ray single crystal structures of **1–*cis*** (left, CCDC: 2288134) and **1–*trans*** (right, CCDC: 2288135). Solvent molecules are omitted for clarity.

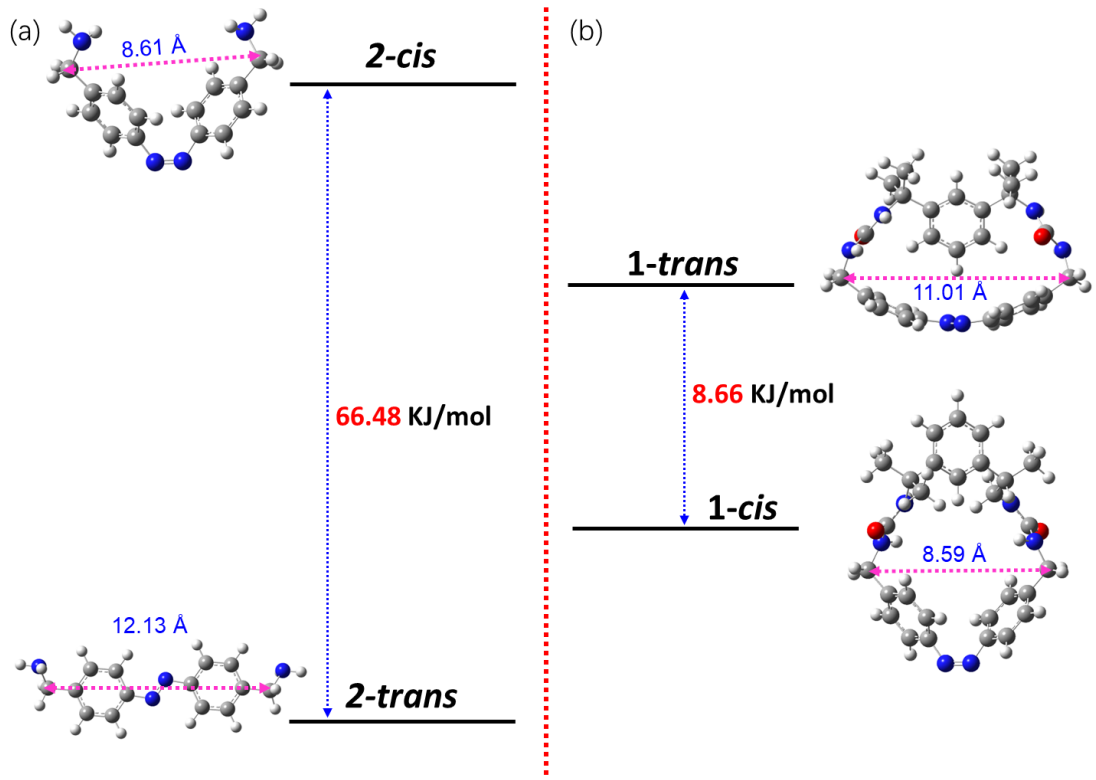

Fig. S22. Relative energies (kJ/mol) of (a) **2-*trans*** and **2-*cis***, (b) **1–*trans*** and **1–*cis.***

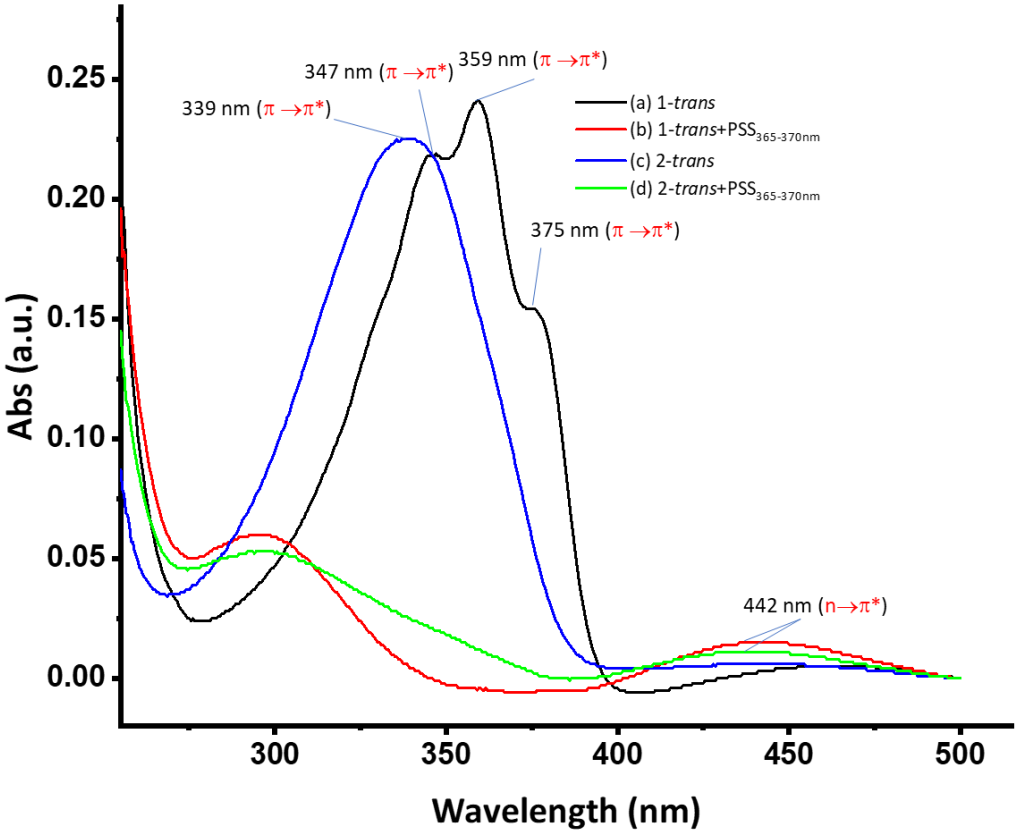

Fig. S23. UV-vis spectrum of (a) **1-trans**, (b) **1-trans** under 365-370 nm light irradiation to PSS, (c) **2-trans**, (d) **2-trans** under 365-370 nm light irradiation to PSS (viz. **1-cis**).

Interestingly, the UV adsorption spectrum of **1-trans** in DMSO showcases three strong absorption peaks (at 347 nm, 359 nm, and 375 nm, respectively) at the range of 250-400 nm, significantly differing from those of other trans isomers of azobenzenes (*e.g.* **2-trans**) with only one absorption peak at 339 nm seen (Fig. S23). This presents the most significant distinguishing spectroscopic feature of **1-trans** in solution. This observation could be rationalized by the fact that the macrocyclic ring strain forced the azobenzene unit to be nonplanar, reducing the conjugation between the azo unit and two connecting benzene rings. However, the absorption spectrum of **1-cis** is somewhat similar to that of other *cis* isomers of azobenzenes (e.g. **2-cis**), indicating that macrocyclization didn't appreciably affect the conjugation of *cis* azobenzene unit compared with other acyclic *cis* azobenzenes.

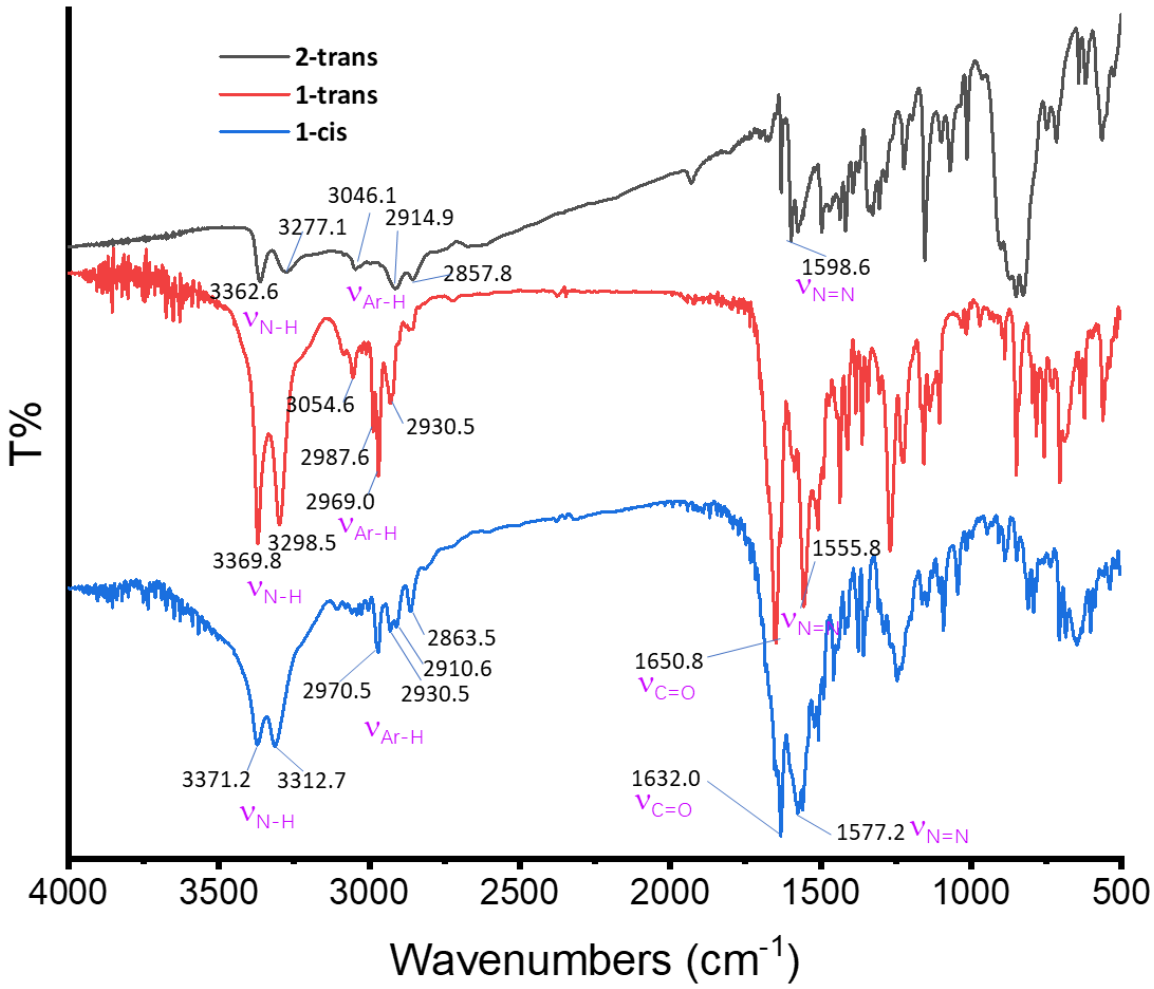

Fig. S24. FTIR spectra of **1-cis** (in light blue), **1-trans** (in red), and **2** (in gray).

Next, we performed Fourier transform infrared spectroscopic (FTIR) analysis to further characterize **1-trans** and **1-cis**. In terms of specifics, characteristic urea NHs peaks (stretching vibration mode) were observed at 3371.2 and 3312.7 cm^{-1} for 1-cis and at 3369.8 and 3298.5 cm^{-1} for 1-trans while the vibration (stretching vibration mode) of urea C=O units is located at 1632.0 cm^{-1} for **1-cis** and 1650.8 $cm^{-1}$for **1-trans** (Fig. S24). This observation could be rationalized by the closer contact of the two urea units of **1-cis**, forming intramolecular hydrogen bonding. More importantly, characteristic peaks at 1577.2 cm^{-1} and 1555 cm^{-1} could be attributed to the N=N vibration mode of the azobenzene units for **1-cis** and **1-trans**, respectively, suggesting that the N=N bond strength can be reduced by macrocyclic ring strain.

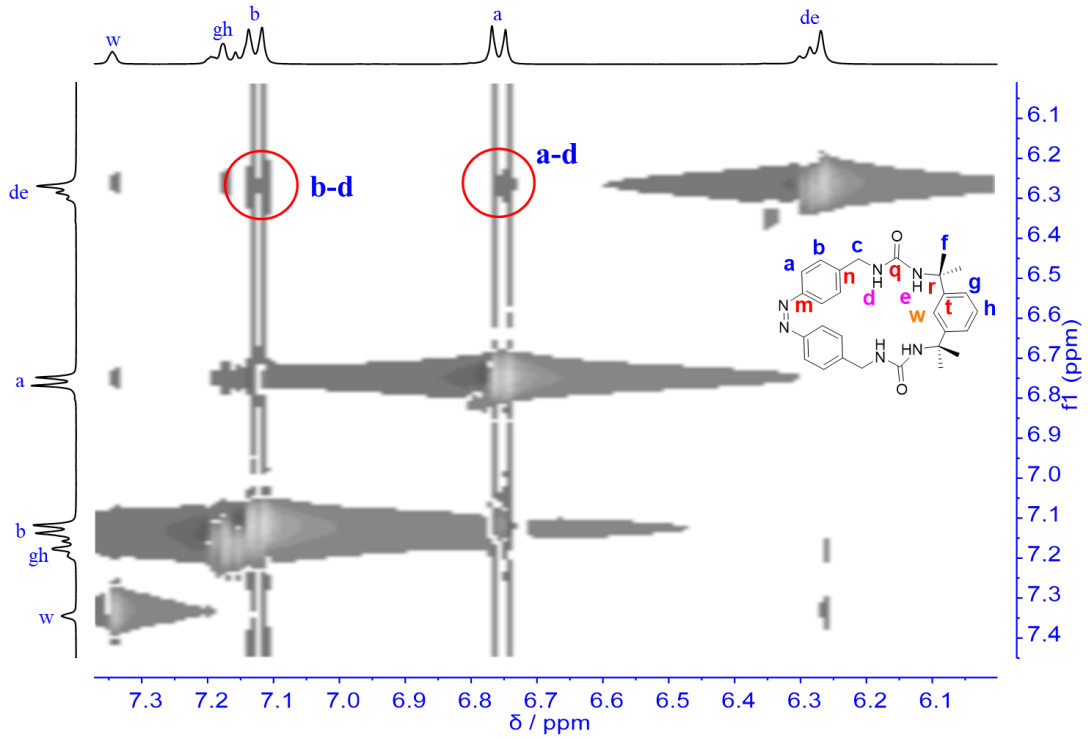

Fig. S25. NOESY spectrum of **1-cis** recorded in DMSO-d_6 at 298 K.

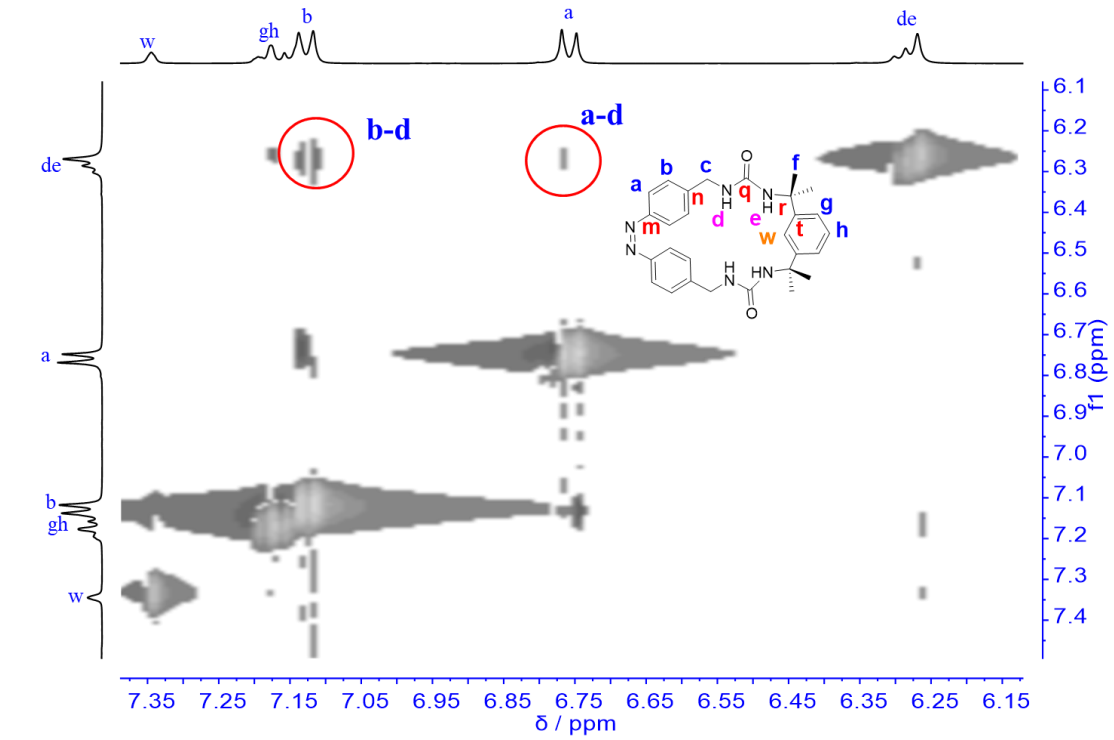

Fig. S26. ROESY spectrum of **1-cis** recorded in DMSO-d_6 at 298 K.

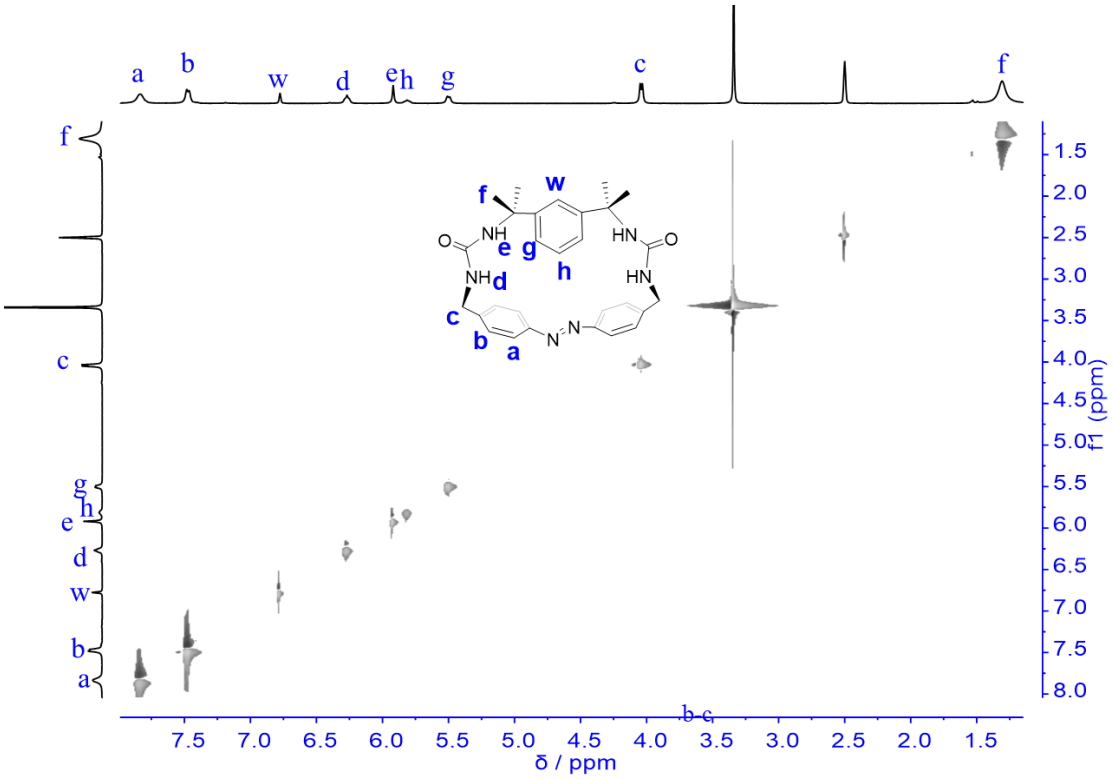

Fig. S27. NOESY spectrum of **1-trans** recorded in DMSO-d_6 at 298 K.

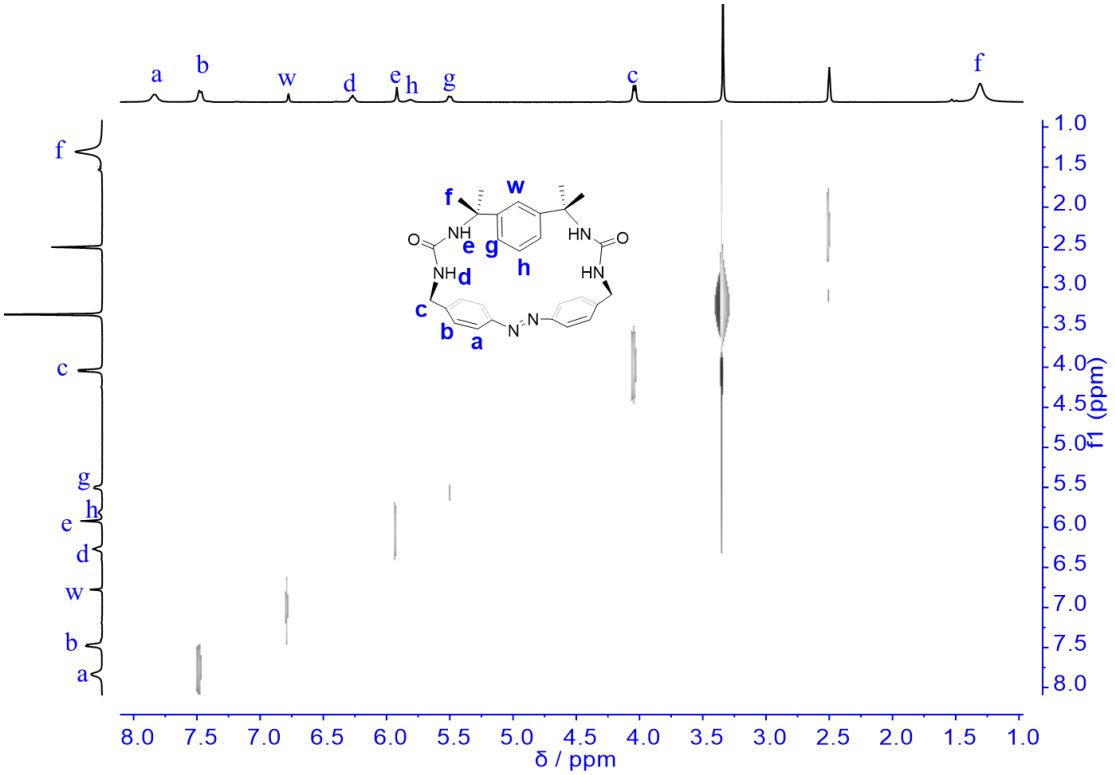

Fig. S28. ROESY spectrum of **1-trans** recorded in DMSO-d_6 at 298 K.

*In order to further study the conformation of **1-cis** and **1-trans**, NOESY experiments were carried out in DMSO-d_6. NOESY correlation of Ar-H**a** (Ar-H**b**) to N-H**d** was found (Fig. S25), indicating that those protons are in close proximity. This observation support the cis configuration of **1-cis**. Such conclusion can be also drawn from similar ROESY experiments (Fig. S26). However, no such NOESY or ROESY correlation of similar protons were seen in the NOESY and ROESY spectra of 1-trans (Figs. S27 and S28).*

4. Stability of receptor 1-*trans*, 1-*cis*, and 2-*cis*

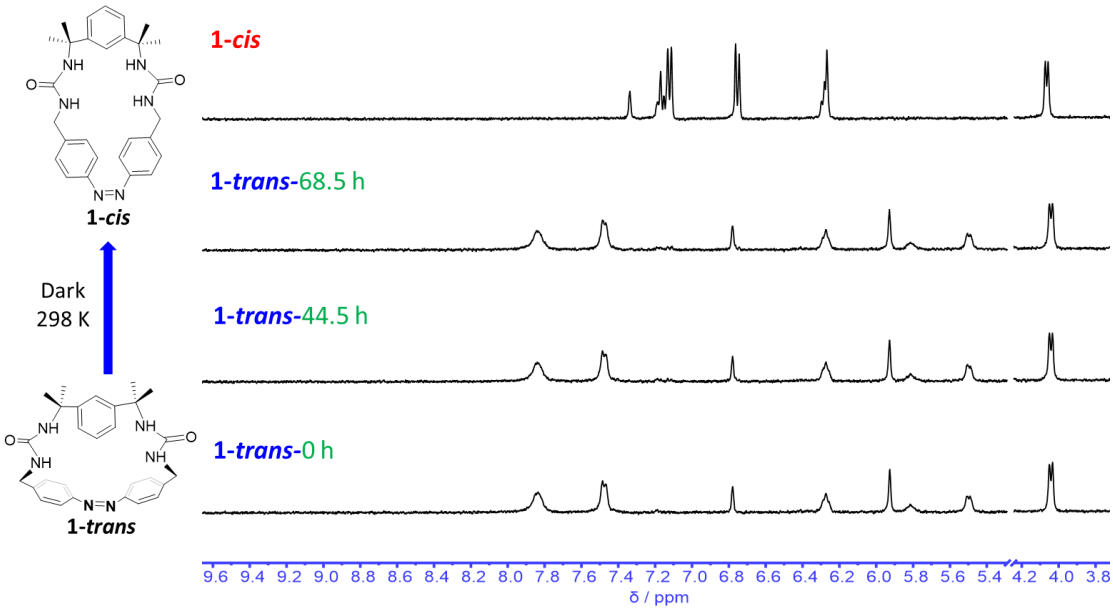

Fig. S29. Partial ^{1}H NMR spectra of **1–*trans*** (1.0 mM in DMSO–d_6) recorded under dark conditions at room temperature after standing for 0 h, 44.5 h, and 68.5 h, respectively.

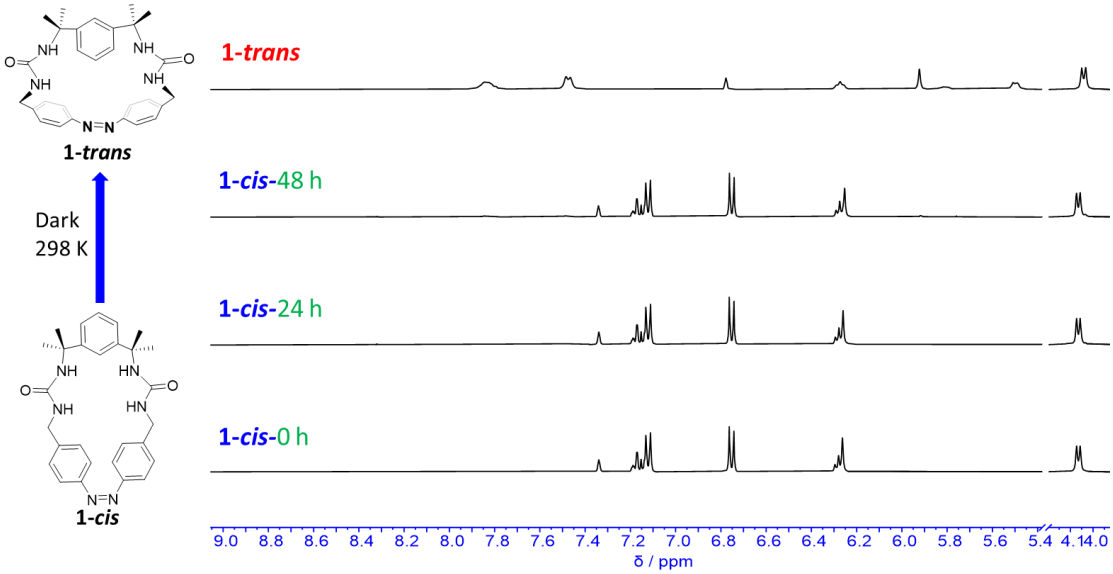

Fig. S30. Partial ^{1}H NMR spectra of **1–*cis*** (1.0 mM in DMSO–d_6) recorded under dark conditions at room temperature after standing for 0 h, 24 h, and 48 h, respectively.

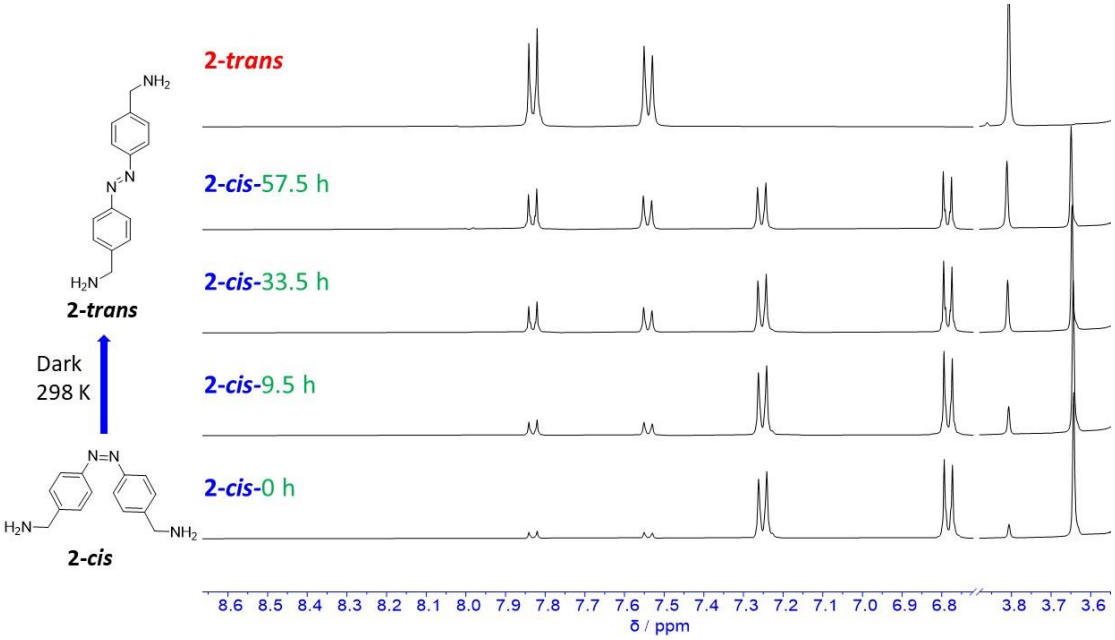

Fig. S31. Partial ^{1}H NMR spectra of **2–*cis*** (1.0 mM in DMSO–d_6) recorded under dark conditions at room temperature after standing for 0 h, 9.5 h, 33.5 h, and 57.5 h respectively.

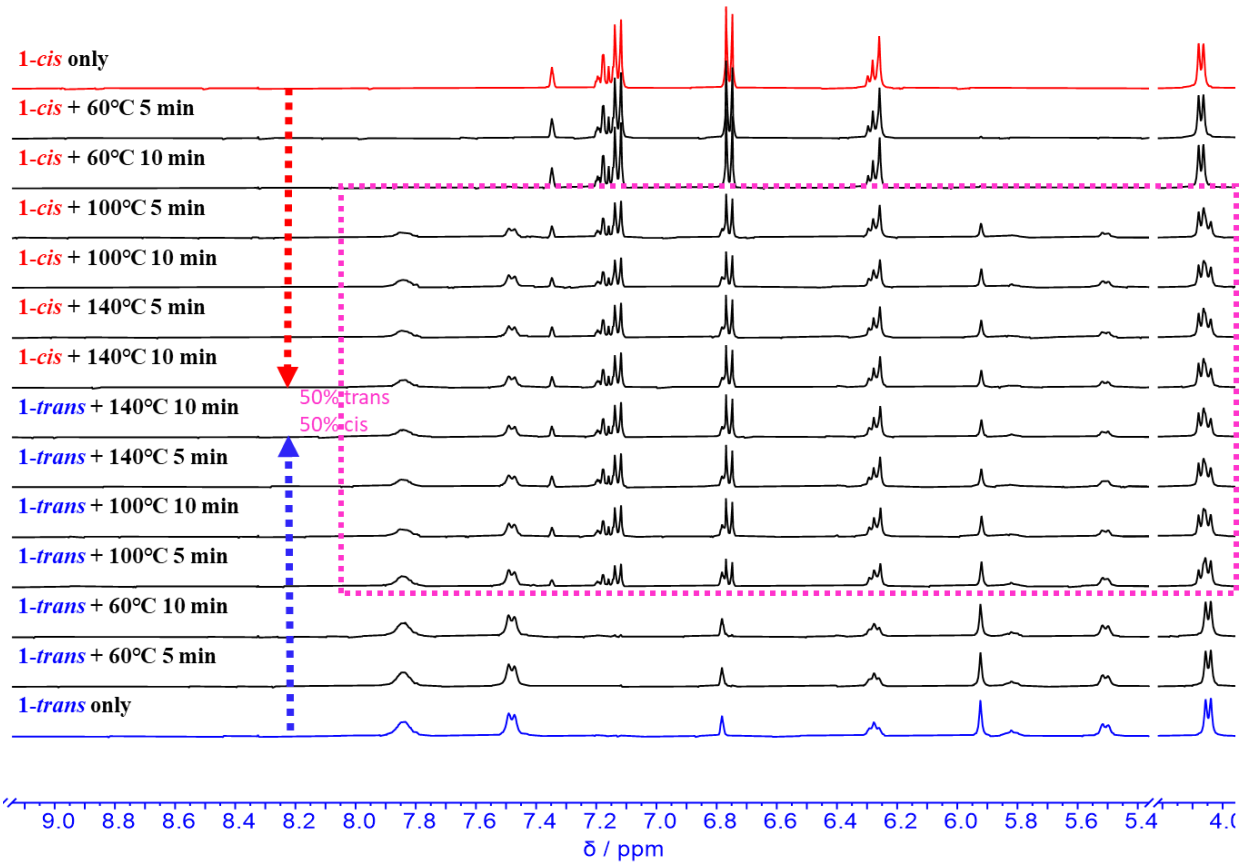

Fig. 31. The *cis-trans* and *trans-cis* isomerization stimulated by thermal stimulus (60℃, 100℃, and 140℃).

We performed extra experiments at different temperature (viz 60℃, 100℃, and 140℃) to study the thermal isomerization (Fig. 32). As a result, like other azobenzene derivatives whose trans isomers are usually unable to thermally isomerize into their corresponding cis ones, **1-trans** was found stable at 60 ℃ (standing for 10 min) without any occurrence of **1-cis** product. Interestingly, unlike linear azobenzenes whose cis isomers can be spontaneously or thermally (e.g. 60 ℃) induced to transform into their corresponding trans isomers, **1-cis** was unable to isomerize into **1-trans** at 60 ℃ within 10 min. Upon increasing the temperature into 100 or 140 ℃, both **1-cis**→ **1-trans** and **1-trans** → **1-cis** isomerization were observed, indicating an unmet thermal isomerization phenomenon in azobenzene chemistry.

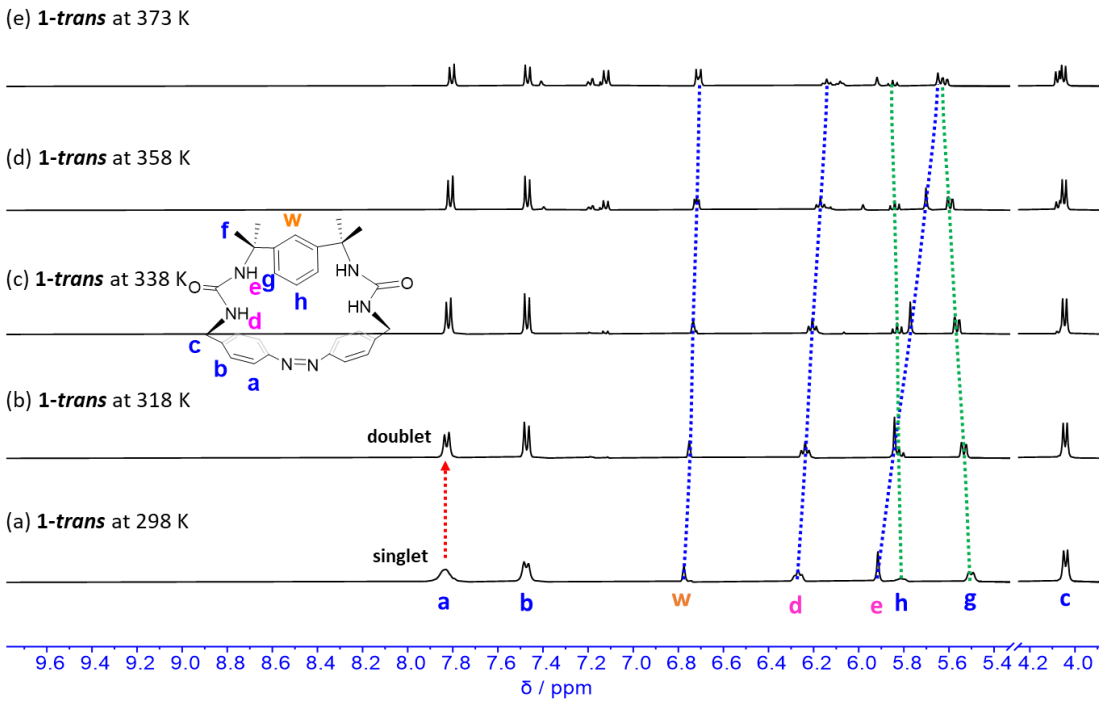

Fig. S33. VT ^{1}H-NMR spectrum (400 MHz, DMSO-d_6) of **1-trans** at 298 K, 318 K, 338 K, 358 K, and 373 K, respectively.

Generally, the structure in the solid state does not have to be necessarily the same in solution. In the case of **1-cis**, all proton resonance signals in the ^{1}H NMR spectrum at 298 K are simplified and well recognized as sharp peaks, indicating that **1-cis** is conformationally flexible and can undergo fluxional behavior. In contrast, most of the proton resonance signals of **1-trans** at 298 K are not split well, giving abnormal broadened peaks due to the ring strain mediated restriction of units in the macrocycle (Fig. S33). However, upon increasing the temperature to 65 ℃, significant improvement of the peak splitting and resolution was observed with only one set of proton resonance signal shown. Continuing increase in the temperature to 100℃ led to the occurrence of a new set of proton resonance signals assignable to **1-cis**, suggesting that, unprecedentedly, thermal stimulus is able to drive the isomerization of **1-trans** into **1-cis**.

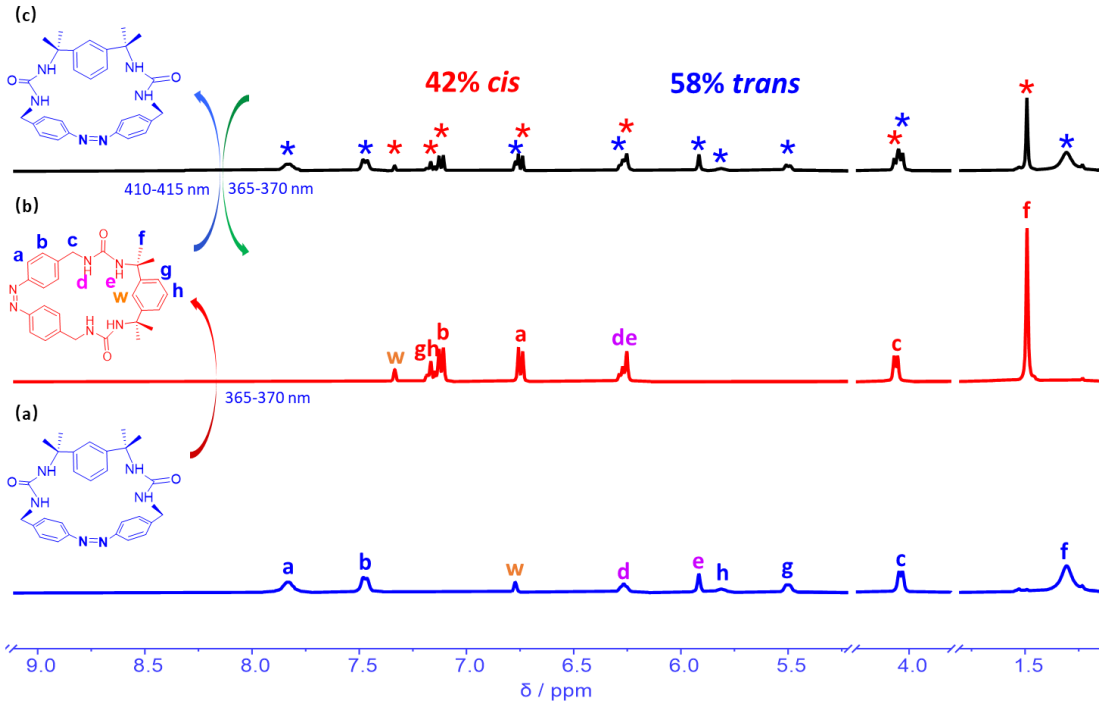

Fig. S34. Partial ^{1}H NMR spectra (DMSO–d_6) of **1–*trans*** (1.0 mM) (a) before and (b) after irradiation with 365–370 nm light and (c) followed by the photoirradiation at 410-415 nm; further followed by 365–370 nm light irradiation back to (b).

5. Binding studies and photo-stimulation

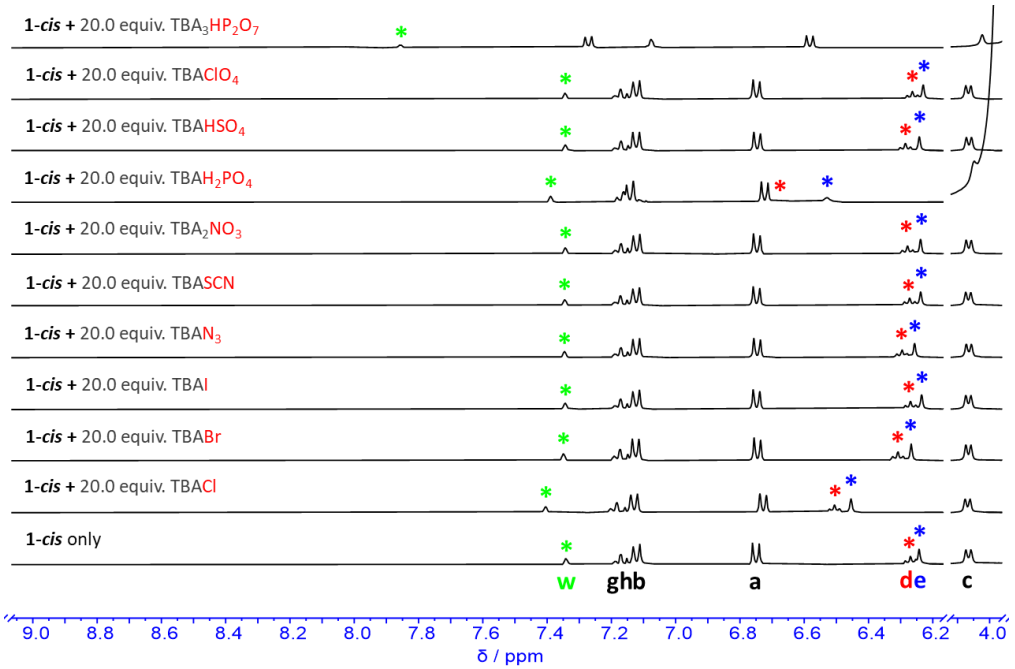

Fig. S35. Selected regions of the 1H NMR spectra (DMSO–d6, 298 K, 400 MHz) of solutions of 1–cis (1.0 mM) recorded in the absence or presence of 20.0 equiv. of Cl^{-}, Br^{-}, I^{-}, N_3^{-}, SCN^{-}, NO3–, $H_2PO_4^{-}$, HSO_4^{-}, ClO_4^{-}, or $HP_2O_7^{3-}$, respectively, as their TBA^{+} salts. Green asteristks: aromatic proton (w); blue asterisks: urea NH (e); red asterisks: urea NH (d) (also refer to Scheme 1).

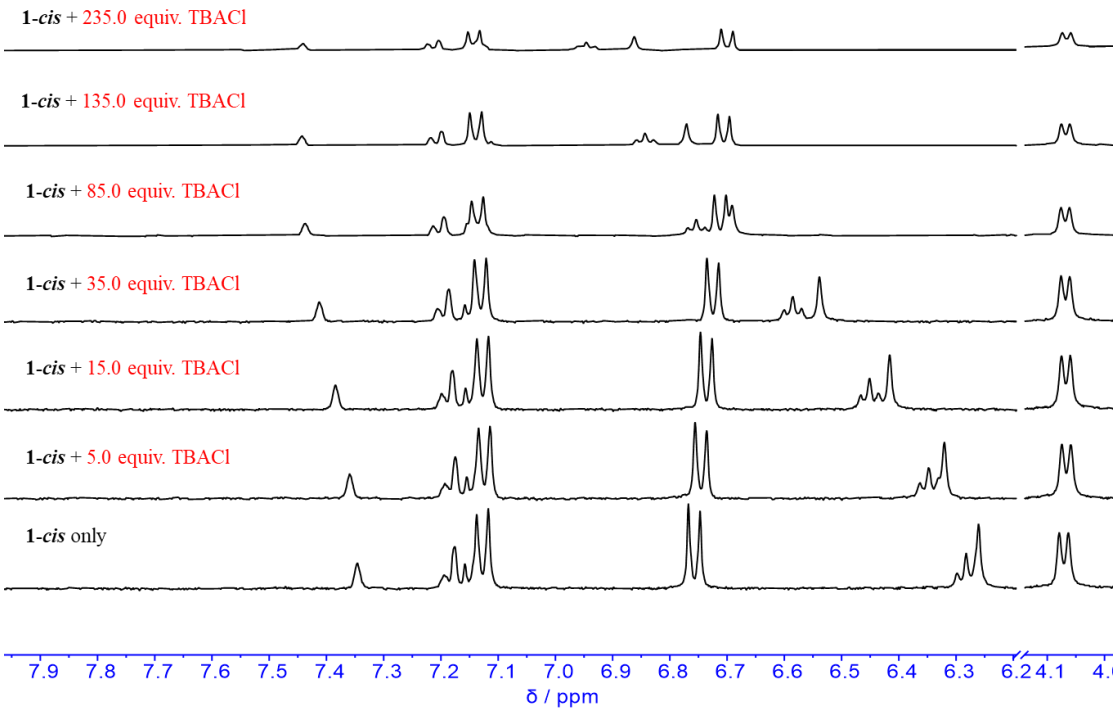

Fig. S36. ^{1}H NMR spectroscopic titration (400 MHz) of receptor **1–*cis*** (1.0 mM) with TBACl in DMSO–d_6 at 298 K.

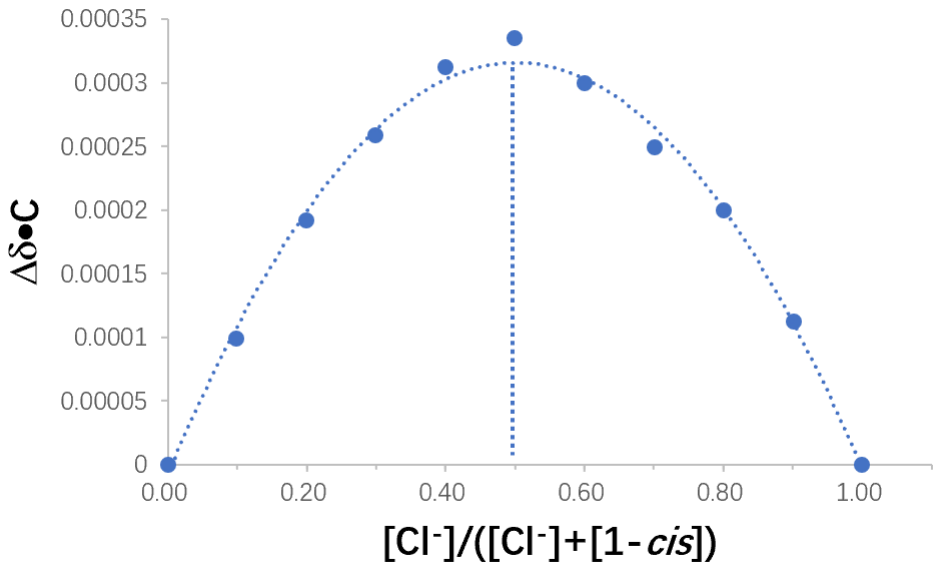

Fig. S37. The Job plot of a 1:1 complex of **1-cis** with Cl^- (as its TBA salt) as measured by ^{1}H NMR spectroscopy carried out in DMSO-d_6. The total concentration of **1-cis** and Cl^- was found to be 2.0 × 10^{-3} M.

Fig. S38. Nonlinear least–square analysis of the ^{1}H NMR binding data corresponding to the formation of **1–*cis***·Cl^{-} complex. The data extracted from Fig. S36 were fitted to a 1:1 binding model to give K_a = (1.74 ± 0.07) ×10 M^{-1}. The residual distribution is shown below the binding isotherm. All solid lines were obtained from non–linear curve–fitting to a 1:1 binding model using the www.supramolecular.org web applet. [6-8]

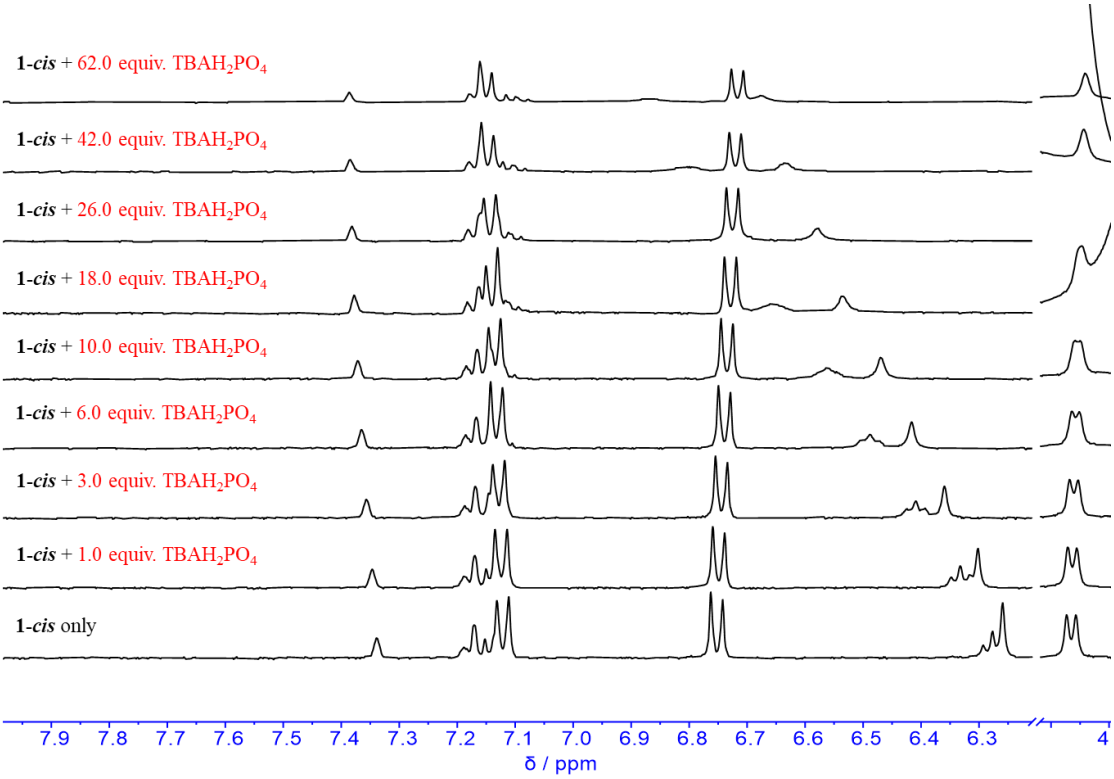

Fig. S39. ^{1}H NMR spectroscopic titration (400 MHz) of receptor **1–*cis*** (1.0 mM) with $TBAHP_2O_4$ in DMSO–d_6 at 298 K.

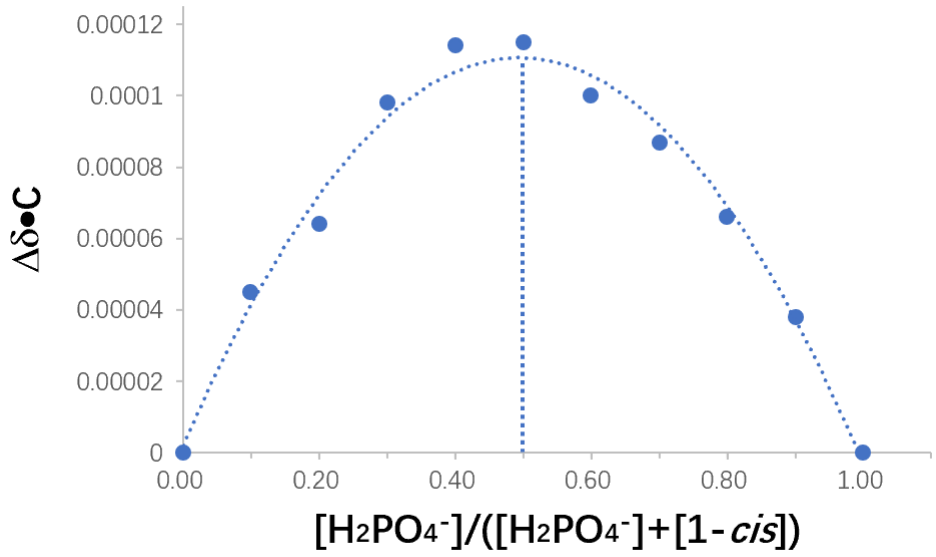

Fig. S40. The Job plot of a 1:1 complex of **1-cis** with $H_2PO_4^-$ (as its TBA salt) as measured by ^{1}H NMR spectroscopy carried out in DMSO-d_6. The total concentration of **1-cis** and $H_2PO_4^-$ was found to be 2.0×10^{-3} M.

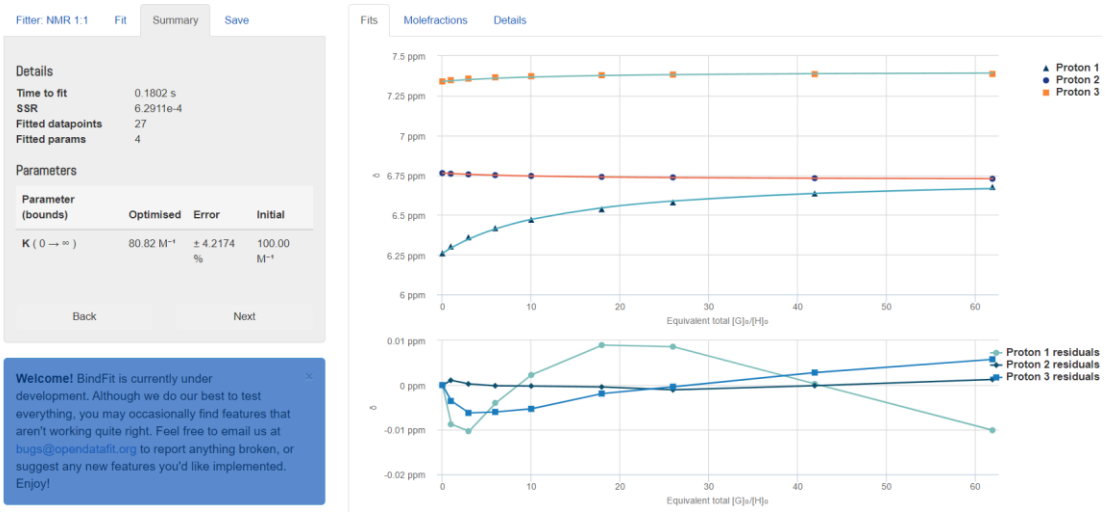

Fig. S41. Nonlinear least–square analysis of the ^{1}H NMR binding data corresponding to the formation of **1–*cis***·$H_2PO_4^-$ complex. The data extracted from Fig. S39 were fitted to a 1:1 binding model to give K_a = (8.08 ± 0.34) ×10 M^{-1}. The residual distribution is shown below the binding isotherm. All solid lines were obtained from non–linear curve–fitting to a 1:1 binding model using the www.supramolecular.org web applet. [6-8]

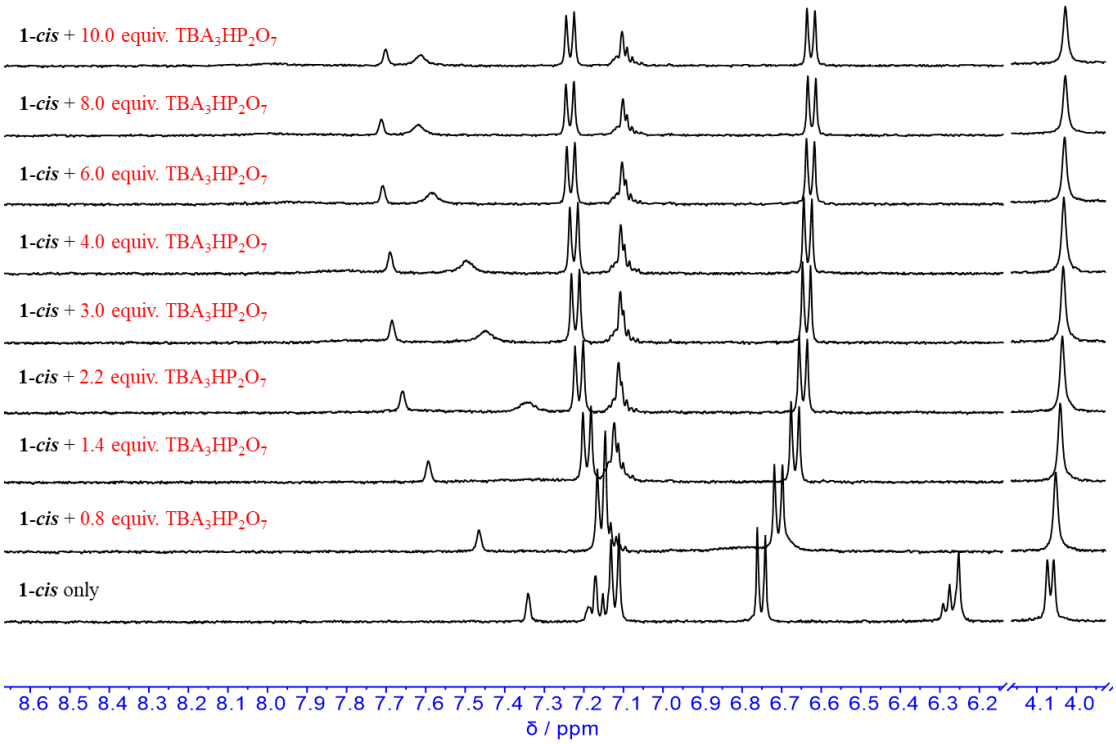

Fig. S42. ^{1}H NMR spectroscopic titration (400 MHz) of receptor **1–*cis*** (1.0 mM) with $TBA_3HP_2O_7$ in DMSO–d_6 at 298 K.

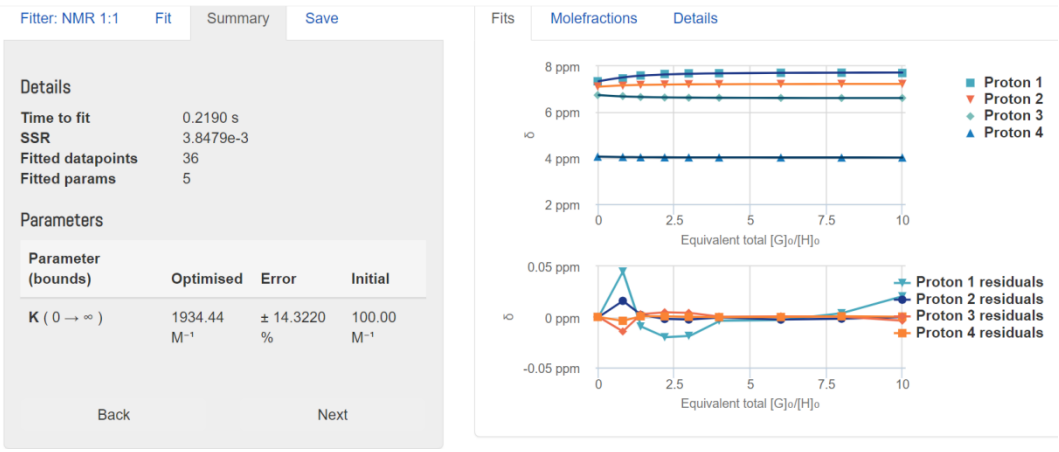

Fig. S43. Nonlinear least–square analysis of the ^{1}H NMR binding data corresponding to the formation of **1–*cis***·$HP_2O_7^{3-}$ complex. The data extracted from Fig. S42 were fitted to a 1:1 binding model to give K_a = (1.93 ± 0.28) ×10^3 M^{-1}. The residual distribution is shown below the binding isotherm. All solid lines were obtained from non–linear curve–fitting to a 1:1 binding model using the www.supramolecular.org web applet. [6-8]

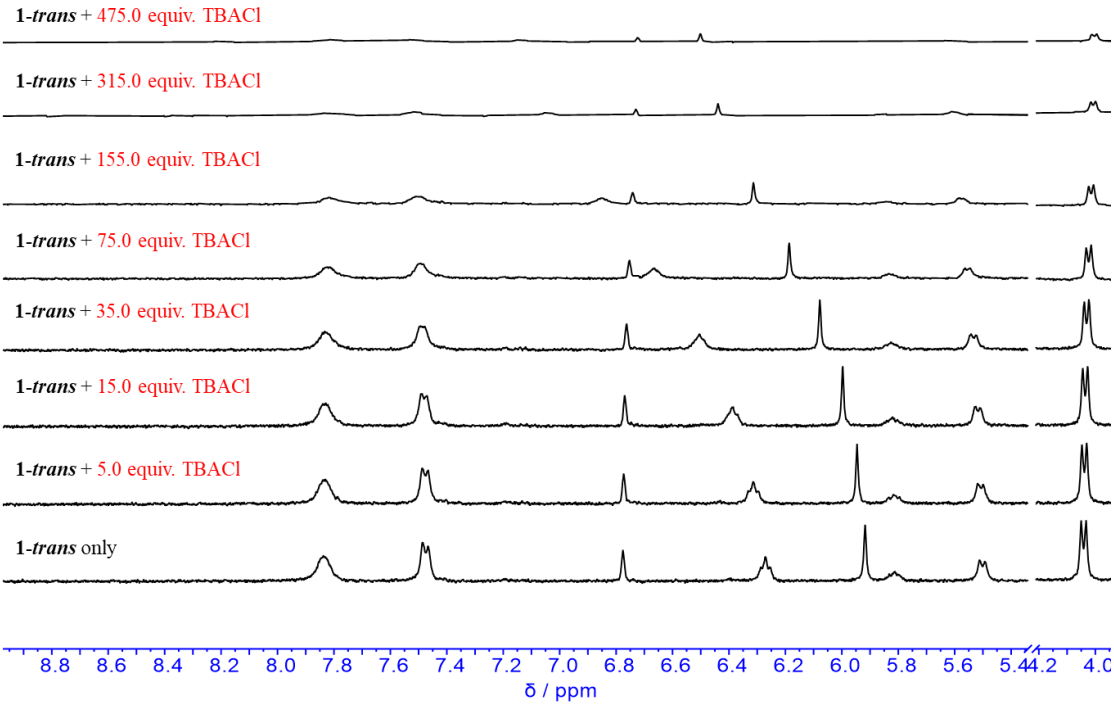

Fig. S44. ^{1}H NMR spectroscopic titration (400 MHz) of receptor **1–*trans*** (1.0 mM) with TBACl in DMSO–d_6 at 298 K.

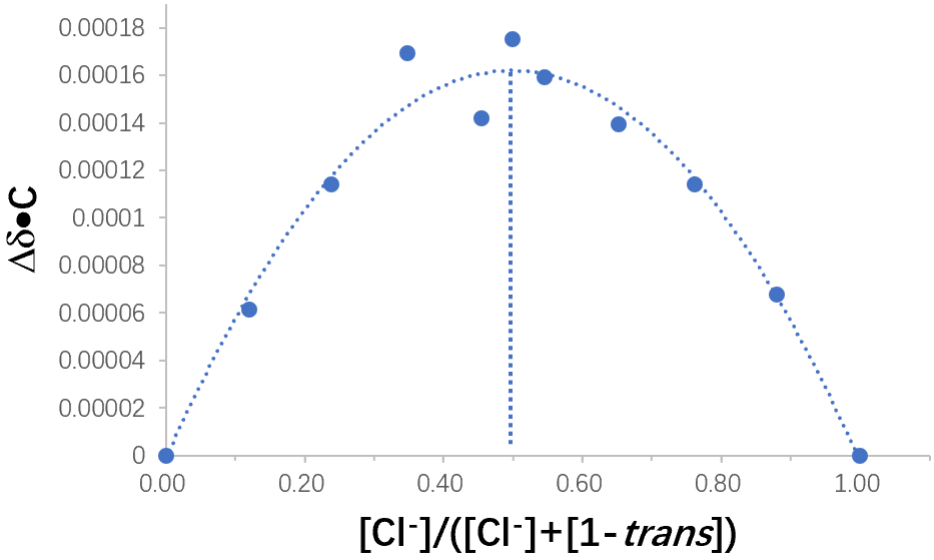

Fig. S45. The Job plot of a 1:1 complex of **1-tran** with Cl^- (as its TBA salt) as measured by ^{1}H NMR spectroscopy carried out in DMSO-d_6. The total concentration of **1-tran** and Cl^- was found to be 2.0 × 10^{-3} M.

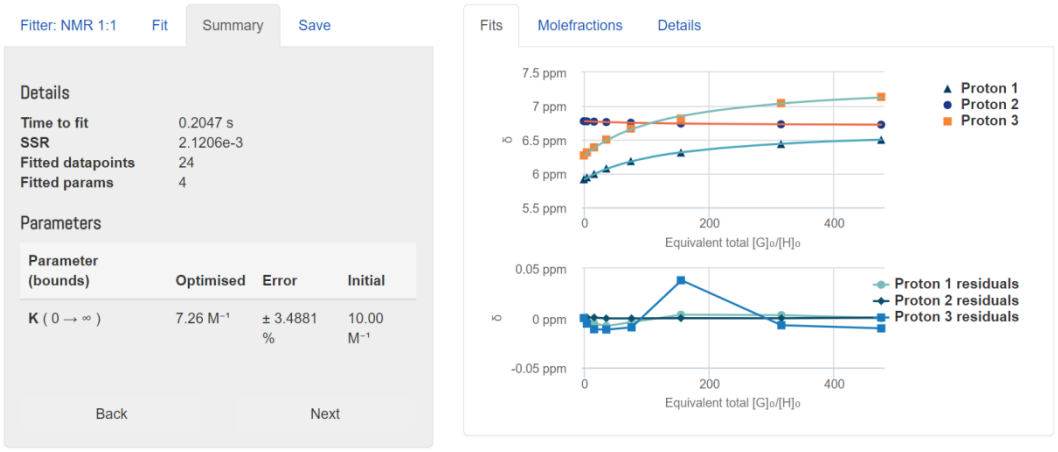

Fig. S46. Nonlinear least–square analysis of the ^{1}H NMR binding data corresponding to the formation of **1–*trans***·Cl^{-} complex. The data extracted from Fig. S44 were fitted to a 1:1 binding model to give K_a = 7.26 ± 0.25 M^{-1}. The residual distribution is shown below the binding isotherm. All solid lines were obtained from non–linear curve–fitting to a 1:1 binding model using the www.supramolecular.org web applet. [6-8]

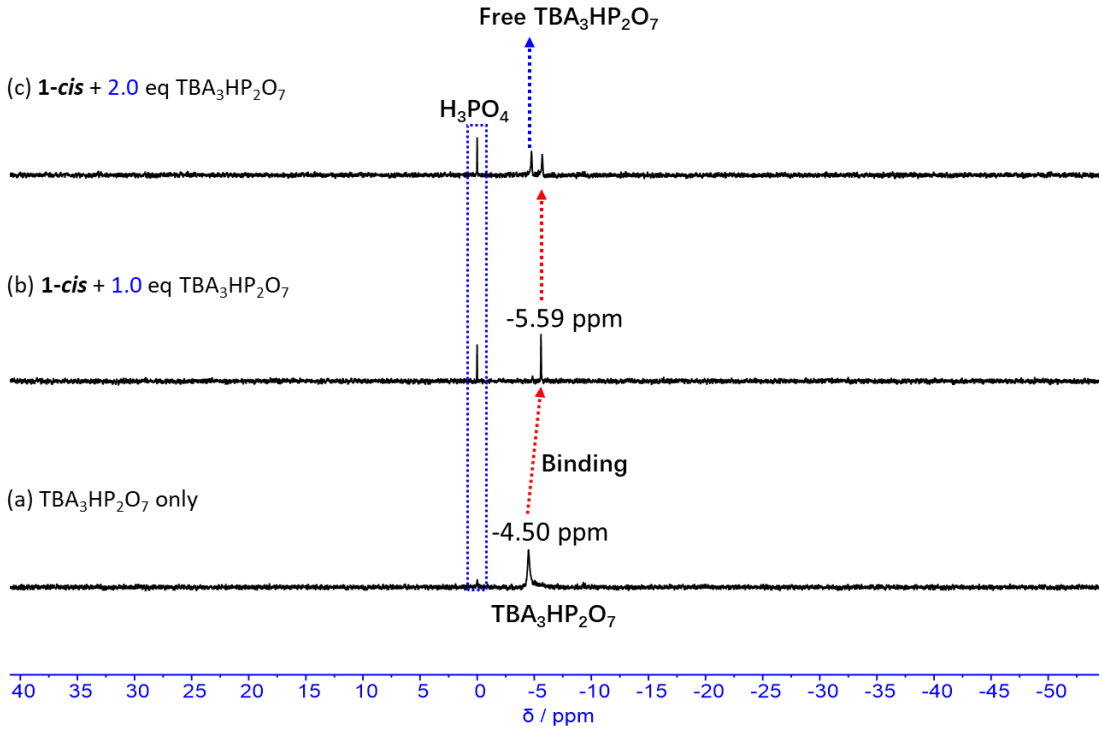

Fig. S47. Stacked ^{31}P NMR spectra of (a) $TBA_3HP_2O_7$; (b) **1-cis** + 1.0 equivalent of $TBA_3HP_2O_7$; (c) **1-cis** + 2.0 equivalents of $TBA_3HP_2O_7$.

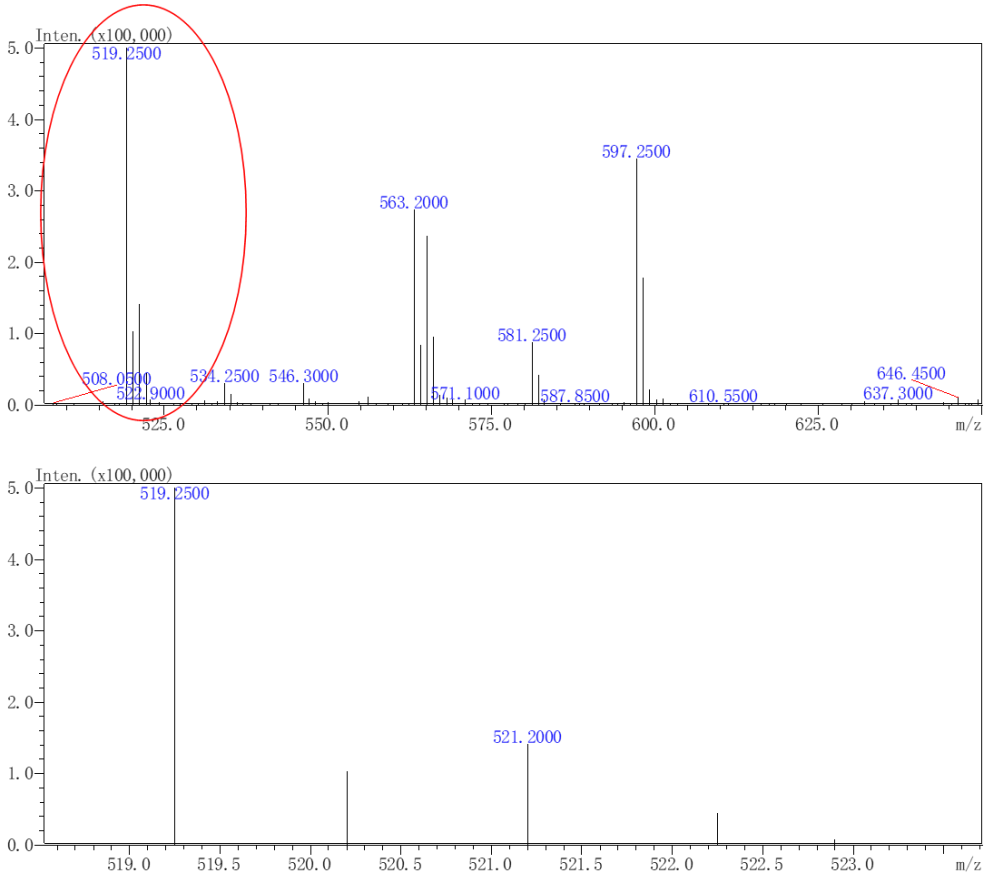

Fig. S48. ESI mass spectrum of **1-cis**·Cl^- complex.

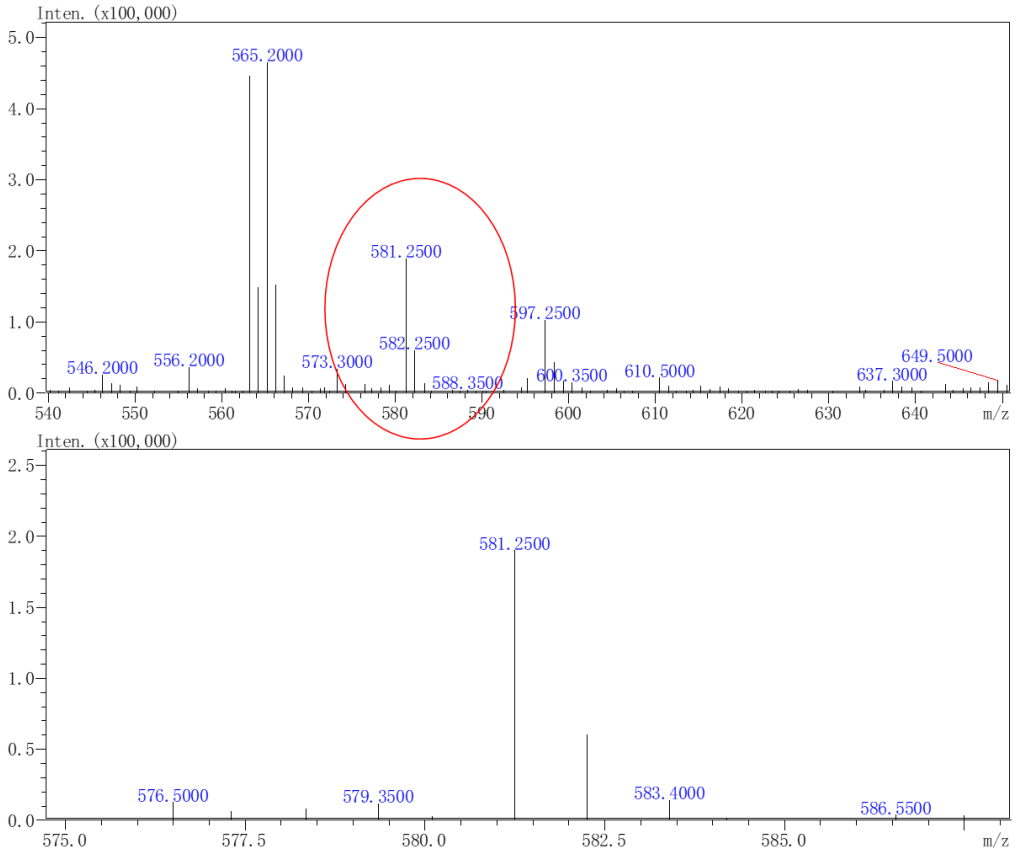

Fig. S49. ESI mass spectrum of **1-cis**·$H_2PO_4^-$ complex.

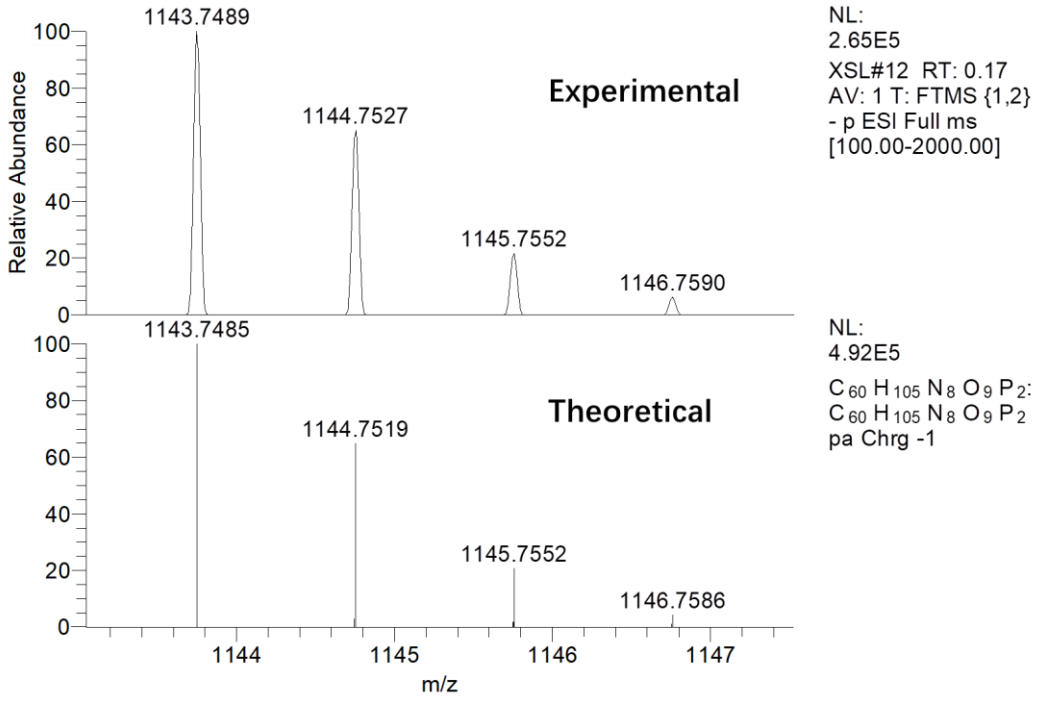

Fig. S50. ESI mass spectrum of **1-cis**·$HP_2O_7^{3-}$ complex, showing the peak of [**1-cis** + 2TBA^+ + $HP_2O_7^{3-}$]$^-$.

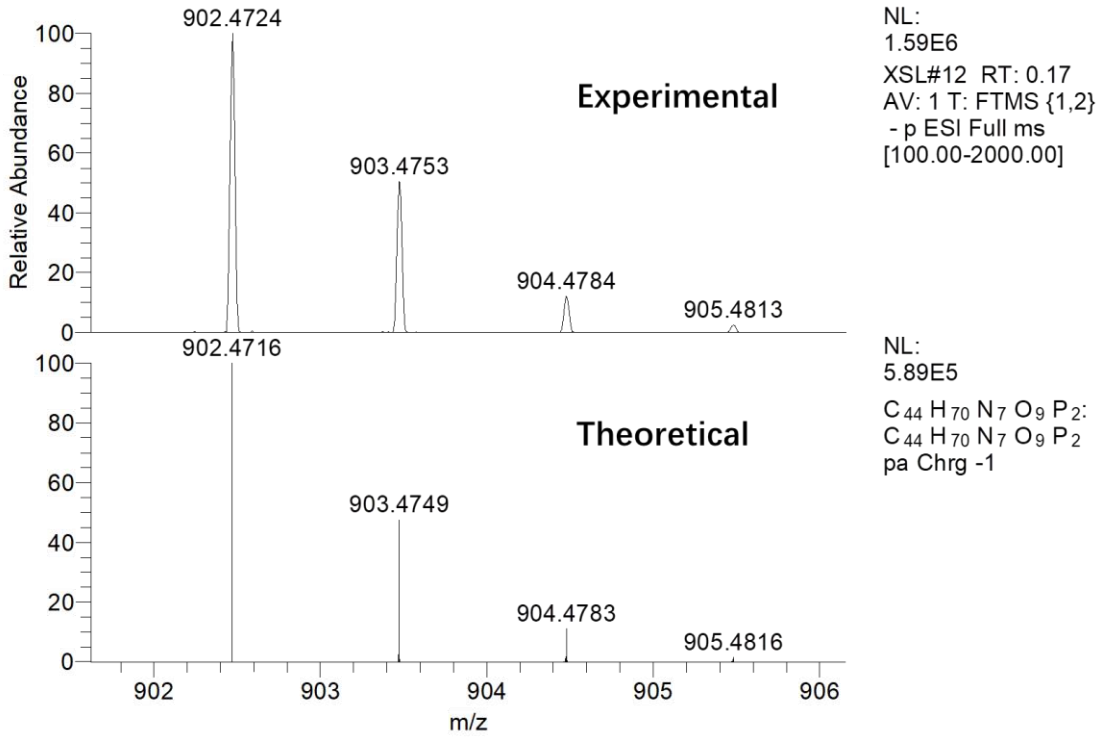

Fig. S51. Expanded ESI mass spectrum of **1-cis**·$HP_2O_7^{3-}$ complex, displaying the peak of [**1-cis** + H^+ + TBA^+ + $HP_2O_7^{3-}$]$^-$.

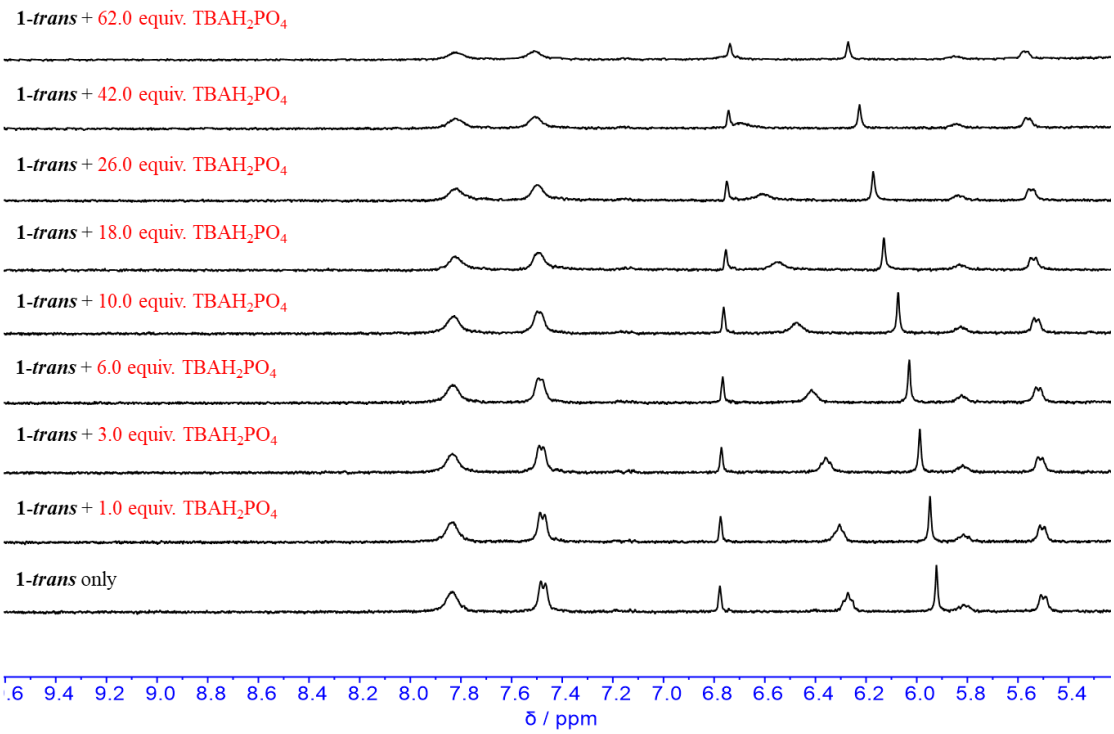

Fig. S52. ^{1}H NMR spectroscopic titration (400 MHz) of receptor **1–*trans*** (1.0 mM) with $TBAH_2PO_4$ in DMSO–d_6 at 298 K.

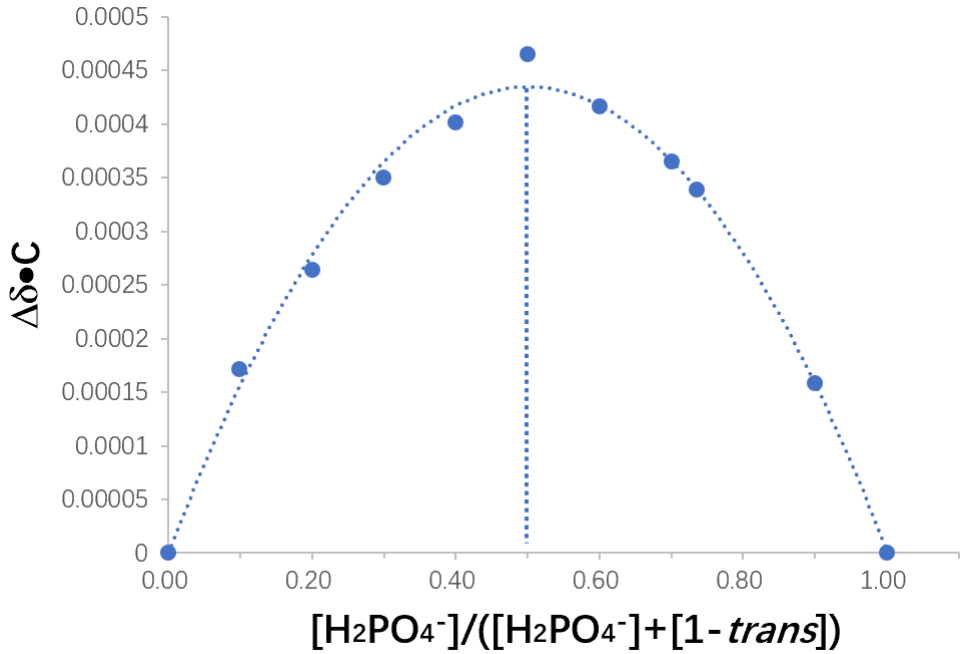

Fig. S53. The Job plot of a 1:1 complex of **1-trans** with $H_2PO_4^-$ (as its TBA salt) as measured by ^{1}H NMR spectroscopy carried out in DMSO-d_6. The total concentration of **1-trans** and $H_2PO_4^-$ was found to be 2.0×10^{-3} M.

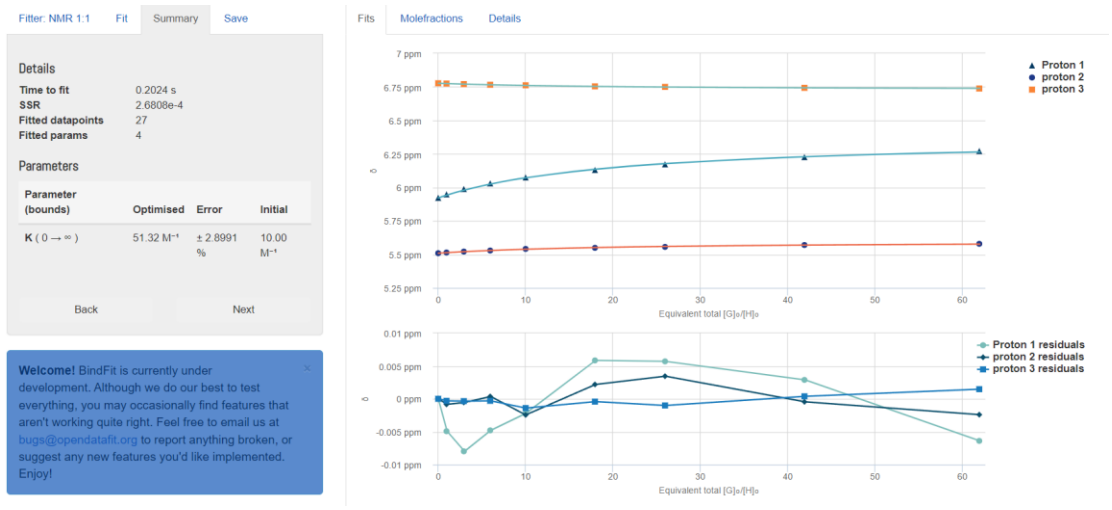

Fig. S54. Nonlinear least–square analysis of the ^{1}H NMR binding data corresponding to the formation of **1–*trans***·$H_2PO_4^-$ complex. The data extracted from Fig. S52 were fitted to a 1:1 binding model to give K_a = (5.13 ± 0.15) ×10 M^{-1}. The residual distribution is shown below the binding isotherm. All solid lines were obtained from non–linear curve–fitting to a 1:1 binding model using the www.supramolecular.org web applet. [6-8]

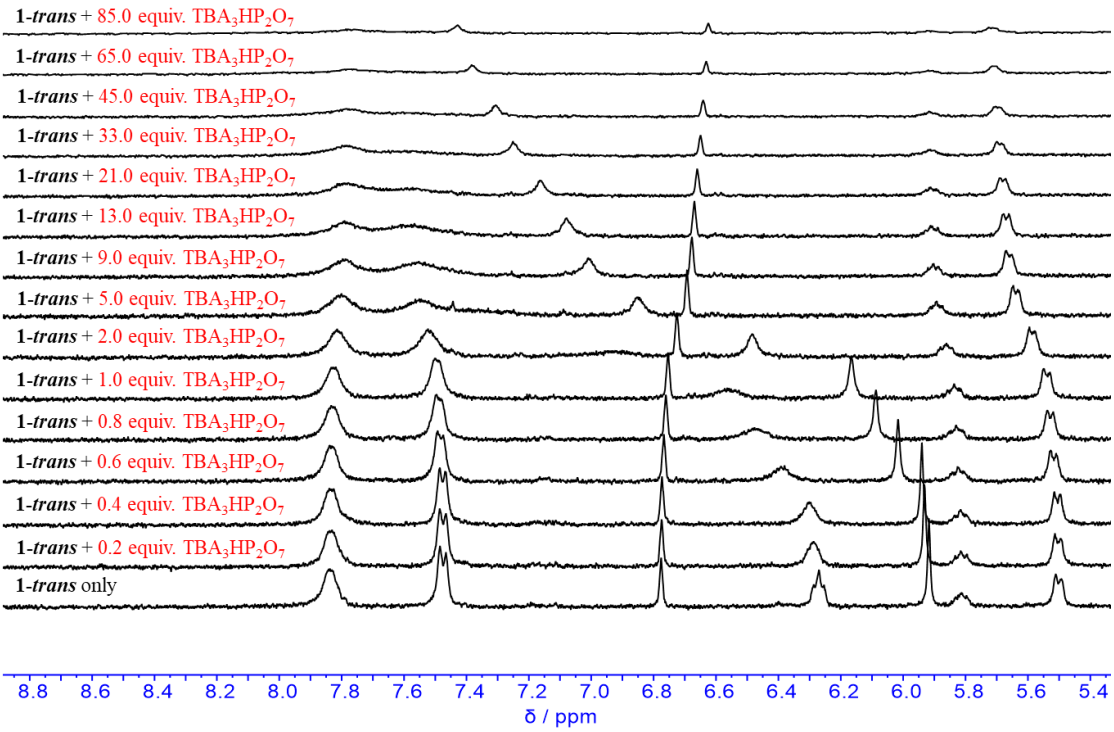

Fig. S55. ^{1}H NMR spectroscopic titration (400 MHz) of receptor **1–*trans*** (1.0 mM) with $TBA_3HP_2O_7$ in DMSO–d_6 at 298 K.

Fig. S56. Nonlinear least–square analysis of the ^{1}H NMR binding data corresponding to the formation of **1–*trans***·$HP_2O_7^{3-}$ complex. The data extracted from Fig. S55 were fitted to a 1:1 binding model to give K_a = (2.82 ± 0.33) ×10^2 M^{-1}. The residual distribution is shown below the binding isotherm. All solid lines were obtained from non–linear curve–fitting to a 1:1 binding model using the www.supramolecular.org web applet. [6-8]

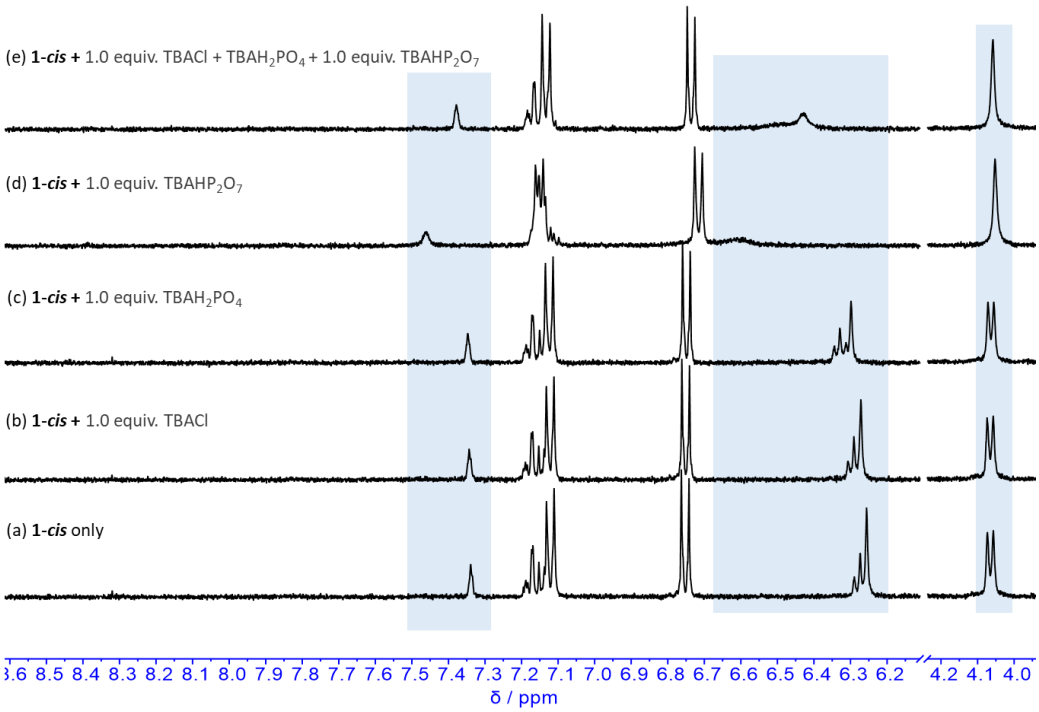

Fig. S57. Partial ^{1}H NMR spectra (400 MHz, DMSO-d_6) of **1-cis** (a) in the absence or in presence of 1.0 equivalent of (b) TBACl, (c) $TBAH_2PO_4$, (d) $TBA_3HP_2O_7$, and (e) equal-molar TBACl, $TBAH_2PO_4$, and $TBA_3HP_2O_7$.

we carried out extra competitive experiments to investigate the selectivity of **1-cis** toward PPi

against other anions. As stated in the main text, **1-cis** displayed very weak or negligible binding of Br^-, I^-, N_3^-, SCN^-, NO_3^-, HSO_4^-, and ClO_4^- (as their tetrabutylammonium (TBA) salts). $H_2PO_4^-$, and Cl^- could be the interfering anionic species. As is shown in Fig. S57, one equivalent of either $H_2PO_4^-$ or Cl^- failed to cause appreciable changes of the chemical shifts of **1-cis** in DMSO-d_6. In contrast, under identical conditions, significant changes in chemical shifts of **1-cis** was observed in the presence of one equivalent of $HP_2O_7^{3-}$, indicating strong interaction between **1-cis** and $HP_2O_7^{3-}$ anion. More importantly, in the presence of one equivalent of equal-molar $H_2PO_4^-$, Cl^-, and $HP_2O_7^{3-}$, similar chemical shifts of **1-cis** were seen, suggesting that **1-cis** has decent selectivity to HPPi over the competitive $H_2PO_4^-$ and Cl^- anions.

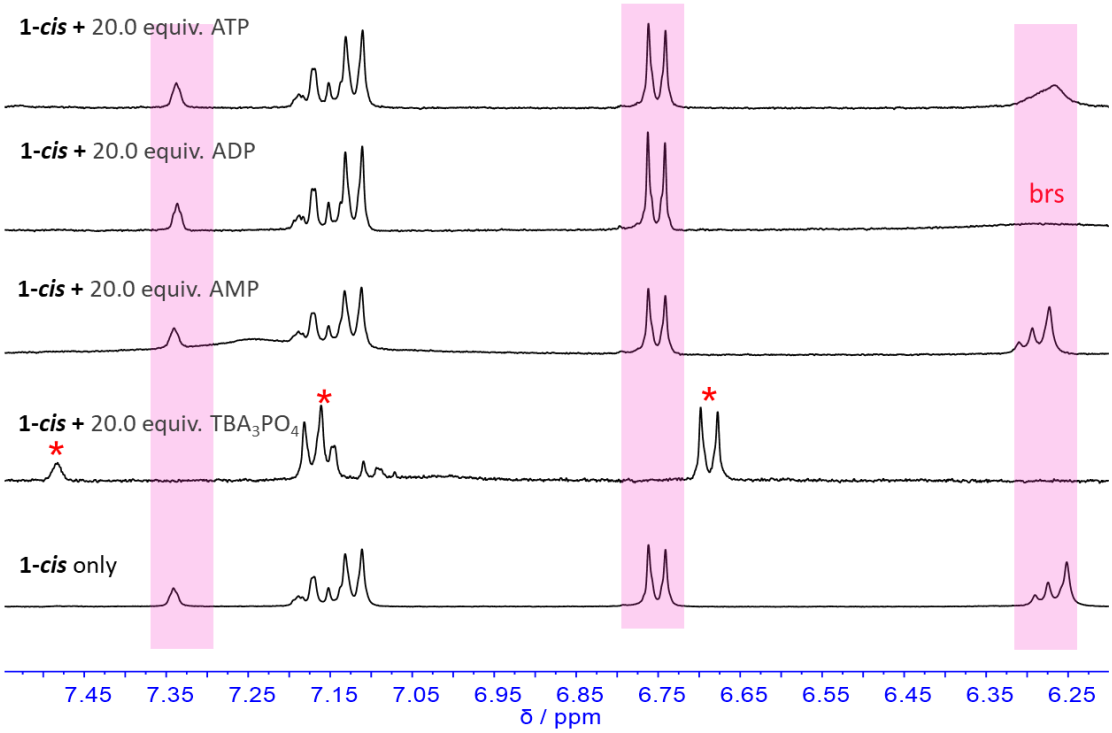

Fig. S58. Partial ^{1}H NMR spectra (400 MHz, DMSO-d_6) of **1-cis** in the absence or in presence of 20.0 equivalent of TBA_3PO_4, AMP, ADP, and ATP, respectively. The concentration of **1-cis** is 1.0 mM.

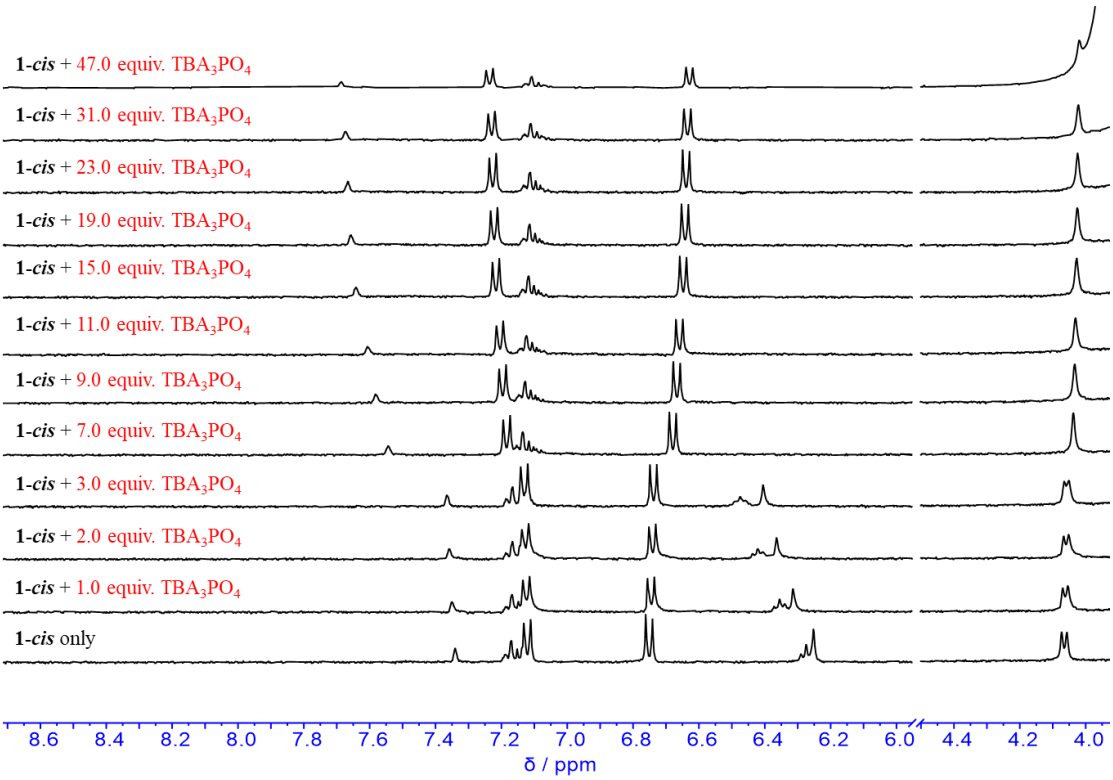

Fig. S59. ^{1}H NMR spectroscopic titration (400 MHz) of receptor **1–cis** (1.0 mM) with TBA_3PO_4 (0-47 equivalents) in DMSO–d_6 at 298 K.

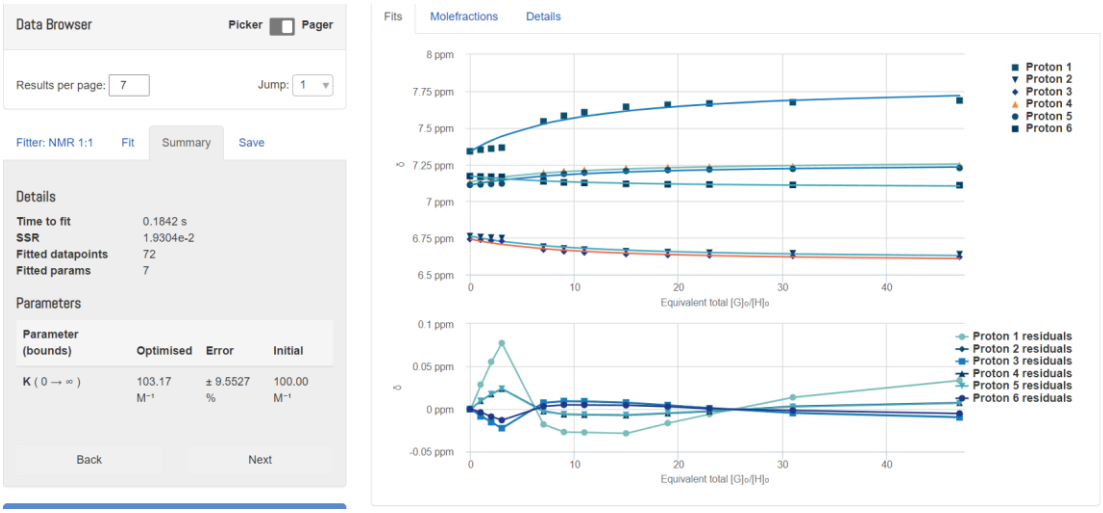

Fig. S60. Nonlinear least–square analysis of the ^{1}H NMR binding data corresponding to the formation of **1–cis**·PO_4^{3-} complex. The data extracted from Fig. S59 were fitted to a 1:1 binding model to give K_a = (1.0 ± 0.1) ×10^2 M^{-1}. The residual distribution is shown below the binding isotherm. All solid lines were obtained from non–linear curve–fitting to a 1:1 binding model using the www.supramolecular.org web applet. [6-8]

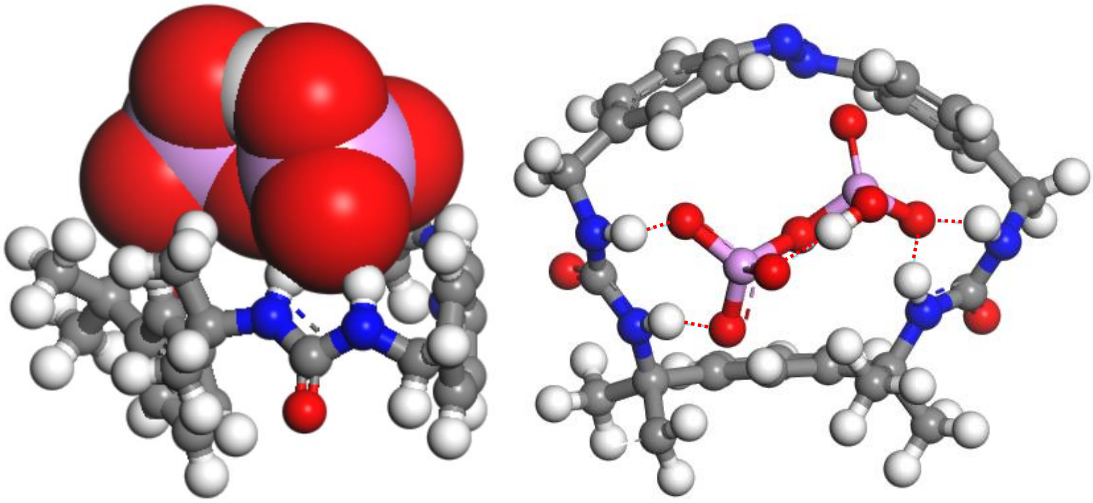

Fig. S61. DFT optimized binding model of **1-*trans*·*H*PPi** complex.

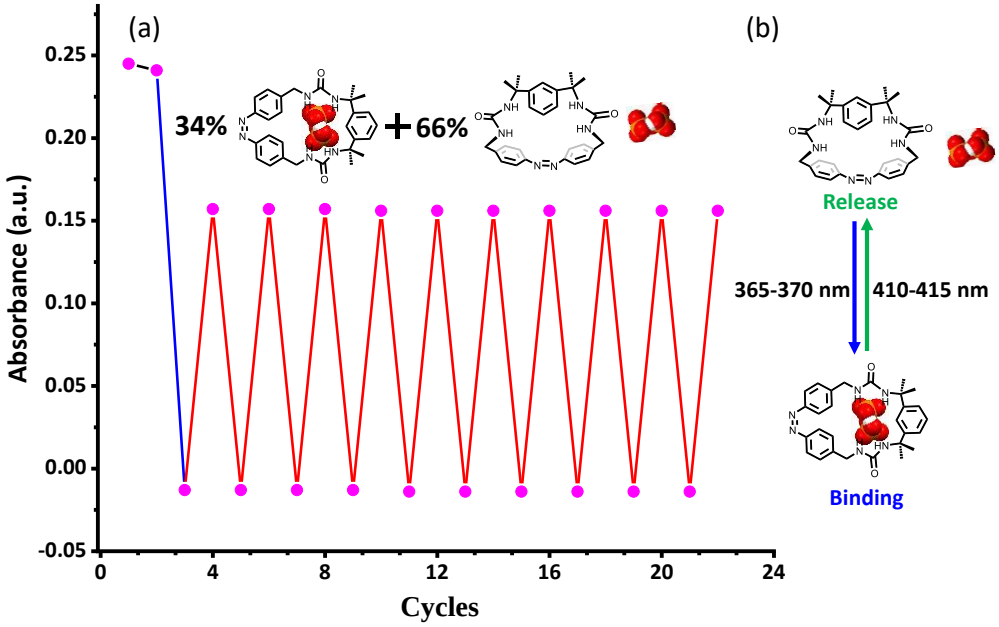

Fig. S62 (a) Switching cycles of **1–*trans*** (10.0 μM in DMSO) in the presence of 20.0 equiv of $TBA_3HP_2O_7$ upon alternating irradiation using 365–370 and 410–415 nm light sources to the PSS state. The absorbance change at 359 nm was monitored during the switching cycles. (b) Insert: Cartoon illustration of the switchable binding and release of PPi anions mediated by UV–Vis irradiation.

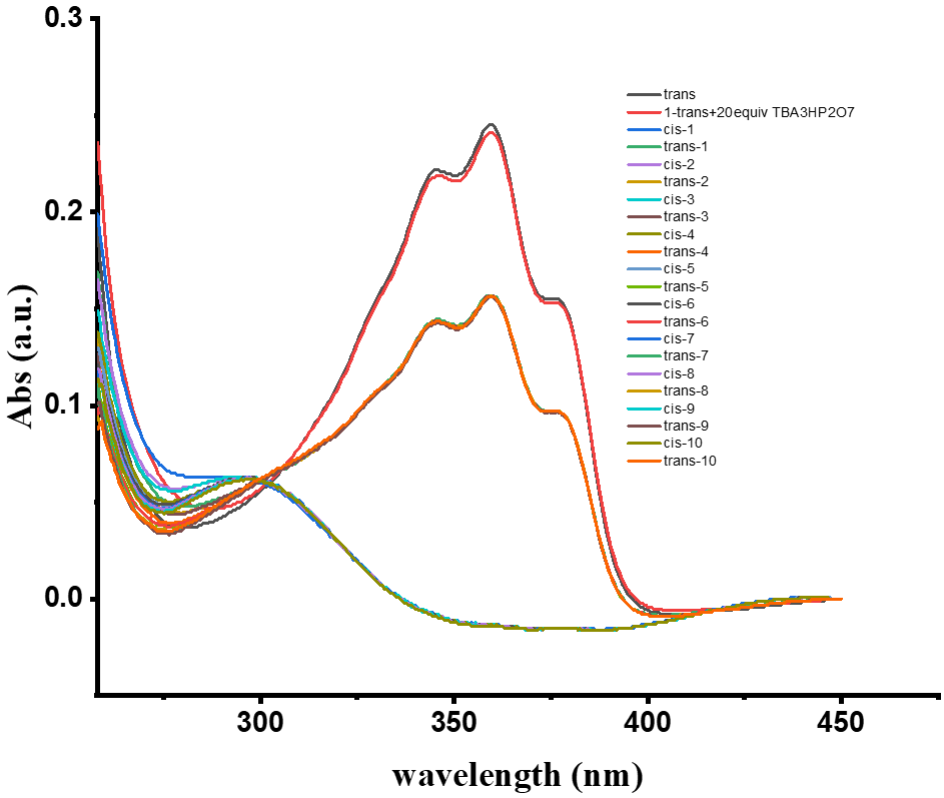

Fig. S63. Reversible photo–switch between **1–*trans*** and **1–*cis*** (10.0 μM) in the presence of 20.0 equiv. of $TBA_3HP_2O_7$ in DMSO monitored by UV–vis spectroscopy.

6. X–ray experimental details

X–ray experimental for 1–*trans*

Single crystals of **1–*trans*** was obtained as red block via the evaporation of a DMF solution of receptor **1–*trans*** in a brown vial. A suitable crystal was selected and the data were collected on a Bruker D8 VENTURE PHOTON 100 CMOS system equipped with a mirror monochromator and a Cu–Kα INCOATEC IμS micro focus source (λ = 1.54184 Å). The crystal was kept at 100.00(10) K during data collection. Using Olex2,[9] the structure was solved with the ShelXT[10] structure solution program using Direct Methods and refined with the ShelXL[11] refinement package using Least Squares minimization. The absolute structure has not been determined based on the data. Tables of positional and thermal parameters, bond lengths and angles, torsion angles and figures are in the CIF file. CCDC deposition number: 2288135.

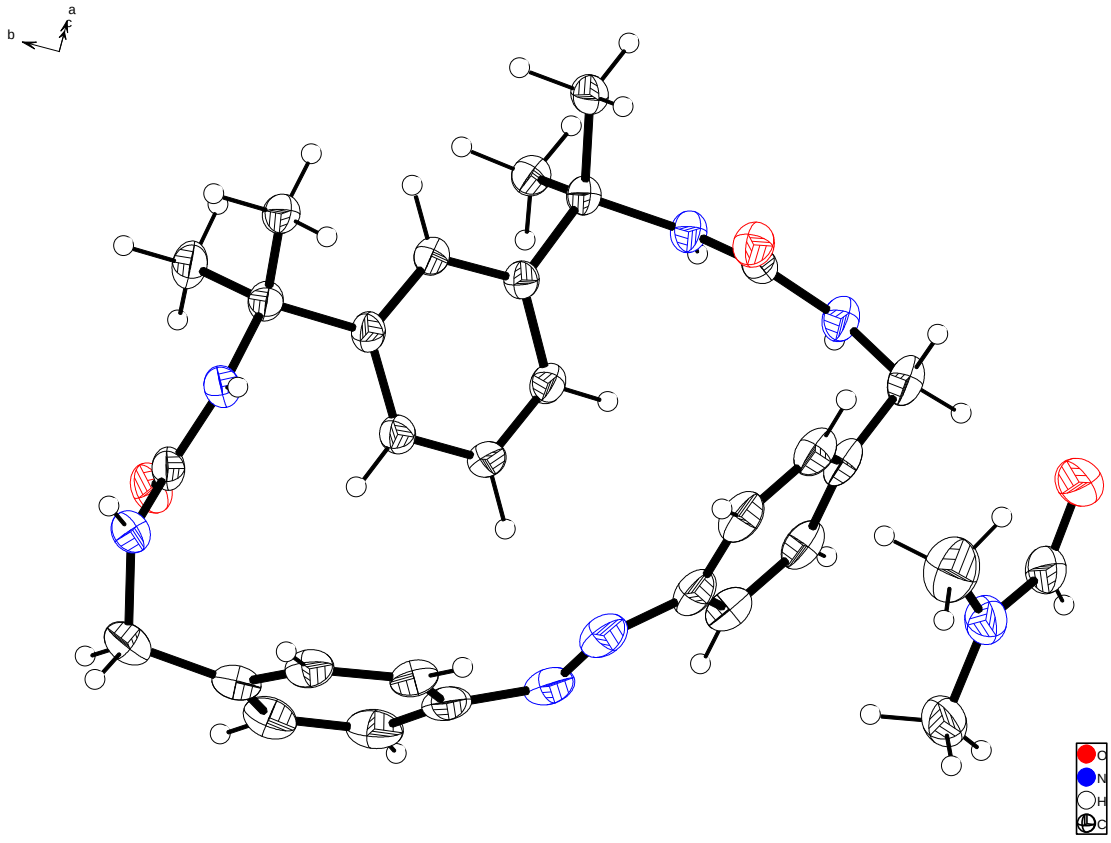

Fig. S64. View of **1–*trans***. Displacement ellipsoids are scaled to the 50% probability level.

Table S1 Crystal data and structure refinement for **1-*trans***.

Identification code	**1-*trans*·*DMF***
Empirical formula	$C_{31}H_{39}N_7O_3$
Formula weight	557.701
Temperature/K	100.00(10)
Crystal system	orthorhombic
Space group	$P2_12_12_1$
a/Å	12.2849(2)
b/Å	14.4216(2)
c/Å	16.5790(2)
α/°	90
β/°	90
γ/°	90
Volume/Å^3	2937.27(7)
Z	4
ρ_{calc}g/cm^3	1.261
μ/mm^{-1}	0.672
F(000)	1195.9
Crystal size/mm^3	0.19 × 0.05 × 0.02
Radiation	Cu Kα (λ = 1.54184 Å)
2Θ range for data collection/°	8.12 to 151.42
Index ranges	-14 ≤ h ≤ 15, -18 ≤ k ≤ 15, -20 ≤ l ≤ 20
Reflections collected	19146
Independent reflections	6009 [R_{int} = 0.0373, R_{sigma} = 0.0356]
Data/restraints/parameters	6009/0/388
Goodness-of-fit on F^2	1.049
Final R indexes [I>=2σ (I)]	R_1 = 0.0370, wR_2 = 0.0943
Final R indexes [all data]	R_1 = 0.0397, wR_2 = 0.0963
Largest diff. peak/hole / e Å^{-3}	0.34/-0.35
Flack parameter	-0.13(10)

X–ray experimental for 1–*cis*

Single crystals of complex **1–*cis*** were obtained as orange block via the evaporation of a DMF solution of receptor **1–*cis*** in a brown vial. A suitable crystal was selected and the data were collected on a Bruker D8 VENTURE PHOTON 100 CMOS system equipped with a mirror monochromator and a Cu–Kα INCOATEC IμS micro focus source (λ = 1.54184 Å). The crystal was kept at 298.00(10) K during data collection. Using Olex2,[9] the structure was solved with the ShelXT[10] structure solution program using Direct Methods and refined with the ShelXL[11] refinement package using Least Squares minimization. The absolute structure has not been determined based on the data. Tables of positional and thermal parameters, bond lengths and angles, torsion angles and figures are in the CIF file. CCDC deposition number: 2288134.

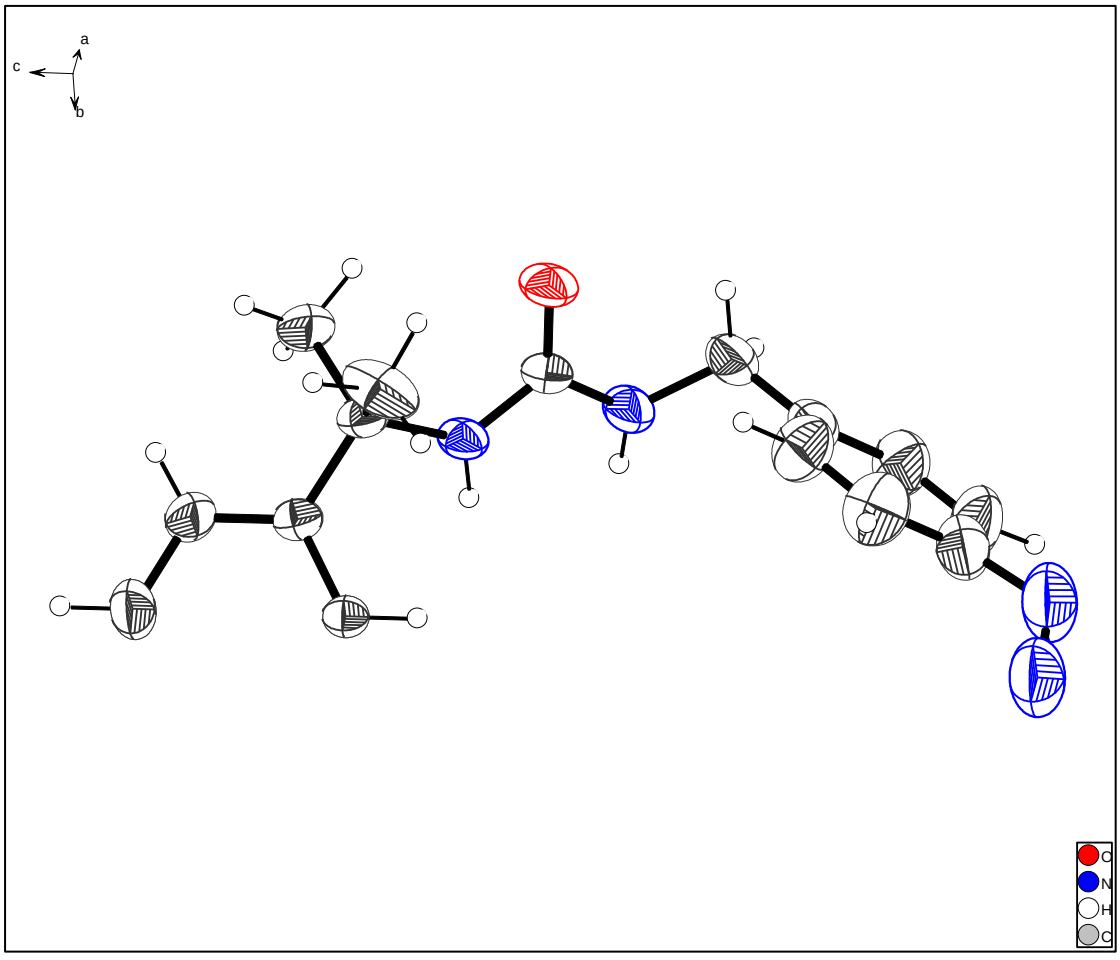

Fig. S65. View of **1–*cis***. Displacement ellipsoids are scaled to the 50% probability level.

Table S2 Crystal data and structure refinement for **1-*cis***.

Identification code	**1-*cis***
Empirical formula	$C_{28}H_{32}N_6O_2$
Formula weight	484.604
Temperature/K	298.00(10)
Crystal system	orthorhombic
Space group	Aea2
a/Å	11.4339(5)
b/Å	9.3891(4)
c/Å	24.5636(11)
α/°	90
β/°	90
γ/°	90
Volume/Å^3	2637.0(2)
Z	0.5
ρ_{calc}g/cm^3	1.210
μ/mm^{-1}	0.634
F(000)	1019.4
Crystal size/mm^3	0.22 × 0.12 × 0.08
Radiation	Cu Kα (λ = 1.54184 Å)
2Θ range for data collection/°	7.2 to 141.04
Index ranges	$-12 \leq h \leq 13, -4 \leq k \leq 11, -29 \leq l \leq 30$
Reflections collected	3578
Independent reflections	1760 [R_{int} = 0.0172, R_{sigma} = 0.0174]
Data/restraints/parameters	1760/1/166
Goodness-of-fit on F^2	1.065
Final R indexes [I>=2σ (I)]	R_1 = 0.0356, wR_2 = 0.0917
Final R indexes [all data]	R_1 = 0.0373, wR_2 = 0.0941
Largest diff. peak/hole / e Å^{-3}	0.11/-0.14
Flack parameter	0.01(18)

7. Geometrical coordinates of the optimized structures

1–*cis*

Cartesian coordinates:

Symbol	X	Y	Z
O	-1.06455900	-4.36958100	0.47914500
N	-1.92296700	-2.40809000	-0.38670000
H	-1.91696700	-1.87792000	-1.24917800
N	0.06284100	-3.28630600	-1.19898500
H	0.18473100	-2.36720700	-1.60586500
C	-3.25189300	-2.44289300	0.27537600
C	-0.99340600	-3.42908800	-0.30470600
C	-3.89853200	-1.07132800	0.01427400
C	-3.15201100	0.09558600	0.22765900
H	-2.10900100	0.00306200	0.51401200
N	5.53596100	-0.73383000	1.15231600
C	2.41256600	-3.15011700	-0.40658200
C	4.45264100	-1.49380200	0.59439600
C	-5.23990100	-0.93573300	-0.36252100
H	-5.85288700	-1.81180200	-0.54131800
C	1.30297700	-4.01918100	-0.97113300
H	1.63688500	-4.48253100	-1.90720000
H	1.04424600	-4.82758300	-0.27988000
C	3.73652900	-3.30487600	-0.83392100
H	3.97474800	-4.06207000	-1.57725800
C	-3.07757800	-2.60613300	1.80207700
H	-2.62489400	-3.57045600	2.03420100
H	-4.05628500	-2.53509600	2.28737700
H	-2.44068600	-1.81204500	2.20319100
C	4.75717200	-2.51141500	-0.31432800
H	5.78700300	-2.64935600	-0.62981300
C	-4.07853400	-3.61804400	-0.27733800
H	-4.27993500	-3.49592600	-1.34742700
H	-5.03505100	-3.71735300	0.24575600
H	-3.51592700	-4.54244500	-0.12950200
C	2.13594900	-2.17711600	0.56338800
H	1.12107000	-2.05660300	0.93104000
C	3.13695800	-1.34734600	1.05338500

H	2.90441400	-0.59179400	1.79565700
C	-5.80458300	0.32973500	-0.50771700
H	-6.84622600	0.42204600	-0.80266400
C	-3.70524600	1.37735000	0.09566900
N	5.51528200	0.51396300	1.20759100
C	2.68268100	2.98853100	-0.75381200
C	4.51109500	1.29322400	0.53706700
C	-5.04926400	1.47924000	-0.27931900
H	-5.51740200	2.45004200	-0.39453900
C	1.62894500	3.82809200	-1.44717900
H	1.48492900	4.77977000	-0.93393100
H	1.93077200	4.03865100	-2.47900600
C	2.87464800	3.06882100	0.63283600
H	2.28394900	3.77529300	1.20858500
C	3.80754600	2.25534700	1.27009400
H	3.98043600	2.33794700	2.33901000
C	3.45076600	2.07409900	-1.48408900
H	3.34201600	2.02393300	-2.56580300
C	4.34781400	1.21905000	-0.85103800
H	4.92862600	0.50503800	-1.42551000
O	-0.39058900	4.22118000	0.43410700
N	-1.61102000	2.45555300	-0.42732000
H	-1.79956100	2.03273200	-1.32803600
N	0.31438100	3.18097300	-1.48760200
H	0.31803900	2.25727000	-1.90379000
C	-2.83370800	2.60791600	0.40570300
C	-0.55685500	3.35170500	-0.41630500
C	-3.53064700	3.93938000	0.07305400
H	-2.83134600	4.75771800	0.25666300
H	-4.41280900	4.09597300	0.70242300
H	-3.84260200	3.97642800	-0.97654800
C	-2.45742900	2.58817200	1.90304900
H	-1.90916800	1.67596600	2.15491600
H	-3.36981800	2.61601000	2.50743900
H	-1.83365700	3.44863700	2.14765800

1–*trans*

Cartesian coordinates:

Symbol	X	Y	Z
O	4.43156600	0.87315200	-1.24186700
O	-4.55253900	0.90267700	-1.03366500
N	3.51317100	1.83161100	0.65108100
N	-3.50196800	1.74278300	0.84695300
N	-5.03066500	-0.00182500	1.01286900
H	-4.64576900	-0.10772700	1.94451900
N	5.08517700	0.12835300	0.82140100
N	0.38633000	-3.53931400	0.36920500
N	-0.32963200	-3.30767700	-0.64258800
C	4.32300000	0.94547000	-0.02042900
C	-0.01294400	2.73727200	0.20716100
H	0.00141800	3.61158900	0.84494100
C	1.20593300	2.20361700	-0.24057000
C	-4.34943200	0.89057600	0.17715400
C	-1.25056400	2.17707900	-0.14821100
C	1.16953100	1.06955800	-1.06136000
H	2.09601300	0.64016200	-1.42609700
C	2.57240700	2.84262200	0.10137900
C	-1.25105100	1.04568100	-0.97272100
H	-2.19150600	0.59897700	-1.27524600
C	-1.71186400	-3.17803400	-0.37153300
C	4.32073300	-2.12394400	0.20218000
C	-3.56263300	-2.78677000	1.12253900
H	-3.98804000	-2.82366200	2.12439100
C	-0.04959000	0.49728200	-1.41464600
H	-0.06455000	-0.39100700	-2.03995000
C	-2.43513100	3.80024200	1.44731900
H	-3.42121800	4.15609400	1.75942800
H	-1.93555200	3.35330400	2.31604800
H	-1.84872800	4.66712100	1.13177800
C	3.58430000	-2.20523500	-0.99181700
H	3.97974700	-1.73756500	-1.88777700
C	1.76474100	-3.27690500	0.17992500
C	-4.28022500	-2.15457600	0.09085100
C	-2.59981900	2.78824100	0.29794600
C	3.16229300	3.51480000	-1.15426100
H	4.13972900	3.95331900	-0.92534000

H	3.28953500	2.80508500	-1.96933400
H	2.48568200	4.31348700	-1.47532200
C	2.46321400	3.91029500	1.20557900
H	2.02521100	3.50354800	2.12577700
H	3.46089400	4.29406300	1.43752600
H	1.84463800	4.75165400	0.88235100
C	2.32081500	-2.77693600	-1.00946900
H	1.71440200	-2.76653200	-1.90765100
C	-2.28988000	-3.29121100	0.90528600
H	-1.69645100	-3.69702400	1.71664300
C	3.81633000	-2.75177300	1.34813700
H	4.39375500	-2.73653000	2.27068700
C	-3.25905100	3.51676000	-0.88991700
H	-3.42174600	2.84752200	-1.73242800
H	-4.22699700	3.93310800	-0.59039200
H	-2.60538500	4.33749800	-1.20296200
C	-2.47801600	-2.68574600	-1.43471200
H	-2.01904900	-2.62726200	-2.41680300
C	5.50610100	-1.18450700	0.30193300
H	5.96211600	-1.01256600	-0.67357500
H	6.27376200	-1.57147000	0.97960900
C	-3.75053200	-2.17006100	-1.20349400
H	-4.29897700	-1.69486300	-2.01000900
C	2.54720500	-3.32280000	1.34101200
H	2.10784000	-3.73559200	2.24394600
C	-5.47179600	-1.27871500	0.42446100
H	-6.13726100	-1.75541400	1.15140900
H	-6.05109000	-1.04238100	-0.46868900
H	3.37134700	1.64859900	1.63530100
H	4.77940100	0.09086600	1.78711100
H	-3.28672200	1.49576300	1.80360700

1–*cis@PPi*

Cartesian coordinates:

Symbol	X	Y	Z
P	0.02747100	0.14138600	2.53829300
O	1.06535000	-0.91853800	2.14796900

O	-1.41795500	-0.34056400	2.38145600
O	0.29349400	3.22446600	3.55026200
O	0.30217500	0.65519400	4.05138700
O	0.21528300	1.48515500	1.65134000
P	0.83628900	3.04318200	2.12358500
O	2.36343300	2.88220200	2.01837700
O	0.24282900	3.92916000	1.02032300
H	0.28701800	1.67620200	4.03146400
O	-1.31719000	-4.51859900	-0.01854300
N	0.37242800	-2.95817300	0.28993000
H	0.69994900	-2.21172100	0.94119000
N	-1.55177600	-2.88427600	1.57091100
H	-1.31029000	-1.89909100	1.86850100
C	1.28321500	-3.56502600	-0.69089000
C	-0.85395500	-3.51000700	0.57106400
C	2.54681700	-2.71029800	-0.93605300
C	2.71191700	-1.38827400	-0.50710900
H	1.96483600	-0.90912500	0.12124700
N	-5.76511500	0.82396000	-1.38829300
C	-3.81191700	-2.18304300	0.89008900
C	-5.08929400	-0.18836200	-0.62668800
C	3.56743400	-3.28516800	-1.71963800
H	3.46689500	-4.30425100	-2.08348700
C	-2.96915700	-3.15529800	1.70139700
H	-3.24770700	-3.06979900	2.75989300
H	-3.14494300	-4.18462200	1.37341600
C	-4.58930700	-1.20006600	1.50671500
H	-4.62663100	-1.15850500	2.59215900
C	0.56797800	-3.68116400	-2.06511600
H	-0.33355700	-4.28545500	-1.96138900
H	1.23677600	-4.13054800	-2.80935500
H	0.29560800	-2.67956400	-2.41283700
C	-5.25689100	-0.23124200	0.75844100
H	-5.83503000	0.54958300	1.24628200
C	1.68071100	-4.97585200	-0.17808900
H	2.25982400	-4.88242200	0.74740600
H	2.28157300	-5.53598800	-0.90519900
H	0.76451700	-5.53529400	0.02346500

C	-3.73677400	-2.18831500	-0.51100100
H	-3.13316700	-2.95147300	-0.99486200
C	-4.35575000	-1.19769300	-1.26441900
H	-4.24599600	-1.17362600	-2.34539600
C	4.70112800	-2.56095600	-2.05877300
H	5.47444700	-3.02083400	-2.67544200
C	3.86573800	-0.64435800	-0.83412800
N	-5.14377800	1.68674800	-2.06107600
C	-1.02271700	2.69514400	-2.29523500
C	-3.72914600	1.90247300	-2.05090100
C	4.85207100	-1.24582500	-1.61774700
H	5.74168400	-0.69226800	-1.89993600
C	0.42485000	3.14364200	-2.47557800
H	0.85999000	2.62916200	-3.34189500
H	0.39987700	4.22056600	-2.72812800
C	-1.93932700	2.92553300	-3.33461500
H	-1.59889100	3.41853300	-4.24599500
C	-3.27238800	2.56474500	-3.20636900
H	-3.99523500	2.77417600	-3.99191900
C	-1.48564200	2.08636400	-1.11996700
H	-0.82025100	1.94301800	-0.27143800
C	-2.81377100	1.67763400	-1.00174500
H	-3.10713700	1.20866000	-0.07124900
O	2.67234000	1.51789400	-2.60859900
N	2.87407700	1.58721700	-0.31435600
H	2.59342600	2.07744300	0.57543400
N	1.30126400	2.89658900	-1.37094500
H	0.99873100	3.26035500	-0.43679900
C	4.06438600	0.75374100	-0.21307800
C	2.31243900	1.95979100	-1.49698800
C	4.31222600	0.54018700	1.30122800
H	4.39220200	1.50612300	1.80772400
H	5.23059400	-0.04578400	1.44566300
H	3.46633700	0.01400600	1.75488600
C	5.26781800	1.50999700	-0.82259700
H	5.10922800	1.66523200	-1.89383900
H	6.22129100	0.98691700	-0.66416500
H	5.33372100	2.48664700	-0.33180500

1–*trans@PPi*

Cartesian coordinates:

Symbol	X	Y	Z
O	4.45711100	-0.29383800	-2.07372500
O	-3.94562700	2.79519600	-1.25829200
N	3.62484200	1.02445300	-0.34716000
N	-2.41304400	2.20053600	0.39298500
N	-4.45715500	1.18721100	0.32127700
H	-3.97119300	0.61612900	1.02545200
N	4.11251500	-1.18451100	0.01890100
N	-1.11392300	-3.98801700	-1.16201200
N	-1.64085400	-3.39837600	-2.14699000
C	4.05949400	-0.15305800	-0.89983100
C	0.98577200	2.65606500	-0.48563200
H	1.26818800	2.45577800	0.54516500
C	1.97969500	2.53379000	-1.47409300
C	-3.59118800	2.11939600	-0.27357400
C	-0.34238200	2.95982900	-0.79786100
C	1.59545500	2.65854200	-2.81172400
H	2.32844900	2.56174400	-3.60756700
C	3.44984800	2.31723300	-1.02162700
C	-0.70885100	3.04762400	-2.15156600
H	-1.75227300	3.20573400	-2.41075400
C	-2.89719000	-2.81926800	-1.79486300
C	2.94505000	-3.23411100	-0.71112900
C	-4.19189100	-1.70727900	-0.08844100
H	-4.33091200	-1.51849100	0.97212000
C	0.25459200	2.88699300	-3.14270800
H	-0.03643100	2.94283100	-4.19202600
C	-0.72764700	3.26848000	1.70765800
H	-1.50069000	3.48123100	2.45448400
H	-0.25863700	2.31412300	1.96057000
H	0.04066800	4.04823700	1.76249400
C	2.49113400	-3.54151800	-2.00591900
H	3.16082200	-3.38747700	-2.85083800
C	0.29691400	-4.02395500	-1.13842800

C	-4.74518400	-0.83868800	-1.04080000
C	-1.38282700	3.24493500	0.31223800
C	4.44074500	2.51269700	-2.18222100
H	5.46174700	2.36527500	-1.81417100
H	4.28317600	1.79352000	-2.98350100
H	4.35171100	3.53898600	-2.56571100
C	3.79023100	3.37874700	0.05825000
H	3.24270600	3.17085600	0.98146000
H	4.86329000	3.33106400	0.28538500
H	3.54668200	4.38940600	-0.29645900
C	1.17090100	-3.92195200	-2.23179900
H	0.78467000	-4.04402500	-3.24043100
C	-3.26464700	-2.66848000	-0.44389100
H	-2.67802400	-3.13194400	0.34273300
C	2.08196500	-3.41790600	0.37540000
H	2.36885500	-3.06574900	1.36516300
C	-2.01960800	4.63213600	0.06891400
H	-2.57748000	4.66727900	-0.86675300
H	-2.71508500	4.86258100	0.88626300
H	-1.23175700	5.39585100	0.05751200
C	-3.55693300	-2.06152200	-2.77236600
H	-3.24159700	-2.15809800	-3.80917700
C	4.27902100	-2.54296200	-0.46960500
H	4.86147700	-2.49306600	-1.39398100
H	4.85828900	-3.10809800	0.27658500
C	-4.46819100	-1.07242000	-2.39326300
H	-4.87940400	-0.40361300	-3.14815800
C	0.76983800	-3.82655800	0.16940000
H	0.05022200	-3.78126900	0.98511800
C	-5.38006900	0.44749500	-0.53602500
H	-6.29519500	0.23068500	0.03838000
H	-5.64997800	1.11008900	-1.36335500
H	3.13058100	0.98293000	0.57507000
H	3.54906000	-1.09325000	0.90283600
H	-2.20720800	1.41466700	1.05193400
P	-1.26276300	-0.89280600	2.53917300
O	-1.42938800	-2.34341500	2.12673300
O	-2.39781500	0.05386700	2.09441800

O	1.34987800	0.10827800	4.20688400
O	-1.08149400	-0.76514000	4.14854200
O	0.13854200	-0.25303500	1.97274100
P	1.67232300	-0.00107000	2.70652500
O	2.56014000	-1.20066900	2.31941400
O	2.16037800	1.30366200	2.03596100
H	-0.13286900	-0.41980300	4.32130000

2–trans

Cartesian coordinates:

Symbol	X	Y	Z
C	-3.97250900	-1.40708400	-0.10648000
C	-2.58777900	-1.54125200	-0.05814900
C	-1.76834300	-0.40672000	-0.06156200
C	-2.35591100	0.86885900	-0.11611500
C	-3.73671800	0.99308000	-0.16926700
C	-4.56535900	-0.14192400	-0.16873000
N	-0.37622000	-0.65805200	-0.00395100
N	0.34772200	0.37361800	0.00209900
C	1.73984800	0.12299500	0.05886700
C	2.56102400	1.25718900	0.06320200
C	3.94587900	1.12866600	0.11597300
C	4.53725200	-0.13869500	0.16422100
C	3.70749000	-1.27167400	0.15182300
C	2.32585500	-1.15276800	0.10447900
C	-6.07115700	-0.00142400	-0.26344000
C	6.04182800	-0.29612800	0.25775500
N	-6.55328400	1.17644200	0.46323000
N	6.74814400	0.78213300	-0.43854900
H	-4.60081700	-2.29468600	-0.09397000
H	-2.11537900	-2.51741000	-0.00853700
H	-1.71152200	1.74067400	-0.11587900
H	-4.20141800	1.97334000	-0.20122200
H	2.08701500	2.23324800	0.02443200
H	4.58572800	2.00472900	0.11218300
H	4.15909000	-2.26127000	0.17725300
H	1.68280800	-2.02535400	0.09313300
H	-6.35200100	0.13658000	-1.31727400

H	-6.53433900	-0.95250600	0.05315700
H	6.34119800	-0.24499200	1.31433300
H	6.31103600	-1.31087900	-0.08485800
H	-7.55514500	1.28397000	0.31987700
H	-6.41307900	1.04437700	1.46346700
H	7.75059200	0.69023100	-0.28919200
H	6.59330200	0.70224800	-1.44218200

2–*cis*

Cartesian coordinates:

Symbol	X	Y	Z
N	-0.62101300	-2.75678500	-0.06679800
C	-3.28712000	0.53770700	0.03870500
C	-1.43082700	-1.57419600	-0.04744200
C	-4.30607700	1.65785700	0.10058800
H	-4.81858000	1.72177500	-0.87536400
H	-5.08250100	1.39918000	0.83432900
C	-3.37874500	-0.45608500	-0.94228100
H	-4.17273600	-0.40665600	-1.68398000
C	-2.48362000	-1.52155500	-0.96763500
H	-2.57636600	-2.31400000	-1.70413900
C	-2.25940800	0.44841500	0.98753200
H	-2.18946400	1.21476800	1.75273300
C	-1.33295900	-0.58775600	0.94505800
H	-0.54241200	-0.64327200	1.68577700
N	0.62118900	-2.75678500	0.06666900
C	3.28707900	0.53788700	-0.03872100
C	1.43096300	-1.57417000	0.04744200
C	4.30594700	1.65812700	-0.10059800
H	4.81852300	1.72199900	0.87531900
H	5.08234100	1.39956000	-0.83441300
C	3.37925200	-0.45632000	0.94180100
H	4.17360600	-0.40715200	1.68312900
C	2.48421000	-1.52185500	0.96714600
H	2.57737200	-2.31461200	1.70326100
C	2.25890800	0.44892700	-0.98707300
H	2.18854200	1.21558900	-1.75192400
C	1.33253900	-0.58732400	-0.94458100

H	0.54160000	-0.64256000	-1.68490500
N	3.70040600	2.91621300	-0.54717000
H	3.05334700	3.25621500	0.16233700
H	4.42082600	3.62771100	-0.65068600
N	-3.70063700	2.91594100	0.54732300
H	-3.05348100	3.25600200	-0.16206700
H	-4.42109500	3.62741200	0.65077200

8. References

1. R. E. Gaussian 09, Frisch, M. J.; Trucks, G. W.; Schlegel, H. B.; Scuseria, G. E.; Robb, M. A.; Cheeseman, J. R.; Scalmani, G.; Barone, V.; Mennucci, B.; Petersson, G. A.; Nakatsuji, H.; Caricato, M.; Li, X.; Hratchian, H. P.; Izmaylov, A. F.; Bloino, J.; Zheng, G.; Sonnenberg, J. L.; Hada, M.; Ehara, M.; Toyota, K.; Fukuda, R.; Hasegawa, J.; Ishida, M.; Nakajima, T.; Honda, Y.; Kitao, O.; Nakai, H.; Vreven, T.; Montgomery, Jr., J. A.; Peralta, J. E.; Ogliaro, F.; Bearpark, M.; Heyd, J. J.; Brothers, E.; Kudin, K. N.; Staroverov, V. N.; Kobayashi, R.; Normand, J.; Raghavachari, K.; Rendell, A.; Burant, J. C.; Iyengar, S. S.; Tomasi, J.; Cossi, M.; Rega, N.; Millam, J. M.; Klene, M.; Knox, J. E.; Cross, J. B.; Bakken, V.; Adamo, C.; Jaramillo, J.; Gomperts, R.; Stratmann, R. E.; Yazyev, O.; Austin, A. J.; Cammi, R.; Pomelli, C.; Ochterski, J. W.; Martin, R. L.; Morokuma, K.; Zakrzewski, V. G.; Voth, G. A.; Salvador, P.; Dannenberg, J. J.; Dapprich, S.; Daniels, A. D.; Farkas, Ö.; Foresman, J. B.; Ortiz, J. V.; Cioslowski, J.; and Fox, D. J., Gaussian, Inc., Wallingford CT, 2009.
2. X. Xu and W. A. Goddard, The X3LYP extended density functional for accurate descriptions of nonbond interactions, spin states, and thermochemical properties, *P. Natl. Acad. Sci. USA*, 2004, **101**, 2673-2677.
3 S. F. Boys and F. Bernardi, The calculation of small molecular interactions by the differences of separate total energies. Some procedures with reduced errors (Reprinted from Molecular Physics, vol 19, pg 553-566, 1970), *Mol. Phys.*, 2002, **100**, 65-73.
4 F. B. van Duijneveldt, J. G. C. M. van Duijneveldt-van de Rijdt and J. H. van Lenthe, State of the Art in Counterpoise Theory, *Chem. Rev.*, 1994, **94**, 1873-1885.
5. J. Liu, X. Jiang, X. Huang, L. Zou and Q. Wang, Photo-responsive supramolecular polymer based on a CB[5] analogue. *Colloid and Polymer Science*, 2016, **294**, 1243-1249.
chemistry, *Chem. Soc. Rev.*, 2011, **40**, 1305-1323.
6 P. Thordarson, Determining association constants from titration experiments in supramolecular
7 D. Brynn Hibbert and P. Thordarson, The death of the Job plot, transparency, open science and online tools, uncertainty estimation methods and other developments in supramolecular chemistry data analysis, *Chem. Commun.*, 2016, **52**, 12792-12805.
8 *Bindfit*. http://app.supramolecular.org/bindfit/, accessed Feb 25, 2023.
9 O. V. Dolomanov, L. J. Bourhis, R. J. Gildea, J. A. K. Howard and H. Puschmann, OLEX2: a complete structure solution, refinement and analysis program, *J. Appl. Crystallogr.*, 2009, **42**, 339-341.
10 G. M. Sheldrick, SHELXT - Integrated space-group and crystal-structure determination, *Acta Crystallogr. A*, 2015, **71**, 3-8.
11 G. M. Sheldrick, Crystal structure refinement with SHELXL, *Acta Crystallogr. C*, 2015, **71**, 3-8.